Synaptic architecture of leg and wing motor control networks in *Drosophila*

Ellen Lesser[1†], Anthony W. Azevedo[1†], Jasper S. Phelps[2^], Leila Elabbady[1], Andrew Cook[1], Brandon Mark[1], Sumiya Kuroda[2^^], Anne Sustar[1], Anthony Moussa[1], Chris J. Dallmann[1], Sweta Agrawal[1^^^], Su-Yee J. Lee[1], Brandon Pratt[1], Kyobi Skutt-Kakaria[3], Stephan Gerhard[2,4], Ran Lu[5], Nico Kemnitz[5], Kisuk Lee[5,6], Akhilesh Halageri[5], Manuel Castro[5], Dodam Ih[5], Jay Gager[5], Marwan Tammam[5], Sven Dorkenwald[6,7], Forrest Collman[8], Casey Schneider-Mizell[8], Derrick Brittain[8], Chris S. Jordan[6], H. Sebastian Seung[6,7], Thomas Macrina[5], Michael Dickinson[3], Wei-Chung Allen Lee[2,9*], John C. Tuthill[1*]

[1]Department of Physiology and Biophysics, University of Washington, WA, USA

[2]Department of Neurobiology, Harvard Medical School, Boston, MA, USA

[3]California Institute of Technology, CA, USA

[4]Aware LLC, Switzerland

[5]Zetta AI LLC, USA

[6]Princeton Neuroscience Institute, Princeton University, NJ, USA

[7]Computer Science Department, Princeton University, NJ, USA

[8]Allen Institute for Brain Science, WA, USA

[9]F.M. Kirby Neurobiology Center, Boston Children's Hospital, Harvard Medical School, MA, USA

^Current address: Neuroengineering Laboratory, Brain Mind Institute & Institute of Bioengineering, EPFL, Lausanne, Switzerland

^^Current address: Optical Biology PhD programme, Laboratory for Molecular Cell Biology, University College London, UK

^^^Current address: School of Neuroscience, Virginia Tech, Blacksburg, VA 24060, USA

†These authors contributed equally

*Correspondence to tuthill@uw.edu, wei-chung_lee@hms.harvard.edu

Abstract

Animal movement is controlled by motor neurons (MNs), which project out of the central nervous system to activate muscles. Because individual muscles may be used in many different behaviors, MN activity must be flexibly coordinated by dedicated premotor circuitry, the organization of which remains largely unknown. Here, we use comprehensive reconstruction of neuron anatomy and synaptic connectivity from volumetric electron microscopy (i.e., connectomics) to analyze the wiring logic of motor circuits controlling the *Drosophila* leg and wing. We find that both leg and wing premotor networks are organized into modules that link MNs innervating muscles with related functions. However, the connectivity patterns within leg and wing motor modules are distinct. Leg premotor neurons exhibit proportional gradients of synaptic input onto MNs within each module, revealing a novel circuit basis for hierarchical MN recruitment. In comparison, wing premotor neurons lack proportional synaptic connectivity, which may allow muscles to be recruited in different combinations or with different relative timing. By comparing the architecture of distinct limb motor control systems within the same animal, we identify common principles of premotor network organization and specializations that reflect the unique biomechanical constraints and evolutionary origins of leg and wing motor control.

Introduction

All motor behaviors, from the simplest postural reflexes to complex locomotor navigation, are produced by patterns of electrical activity in motor neurons (MNs), which project axons from the central nervous system to excite muscles (Sherrington, 1906). A single MN and its target muscle fibers comprise a motor unit. Because animal bodies are controlled by large numbers of motor units with overlapping functions, many behavioral tasks can be accomplished using different combinations of motor unit activation. How the nervous system selects one pattern of motor unit activation among the many possible options has been referred to as the "degrees of freedom problem" (Bernshteĭn, 1967). The degrees of freedom problem is particularly acute for limb motor control systems that involve coordination of multiple joints (Hug et al., 2023). Previous work has used analysis of limb biomechanics, movement kinematics, and electrophysiological recordings to identify patterns of motor unit coordination (Lobato-Rios et al., 2022; Marshall et al., 2022; Ting and Macpherson, 2005). However, the space of possible motor unit activations is ultimately constrained by the anatomy and connectivity of premotor neural circuits (Hodson-Tole and Wakeling, 2009). Thus, determining the wiring logic of premotor circuits would provide fundamental insight into how nervous systems flexibly coordinate motor units to accomplish diverse motor tasks.

Recent progress in volumetric electron microscopy and image segmentation has made it possible to reconstruct complete wiring diagrams from small nervous systems. Connectomes now exist for the nematode *C. elegans* (Cook et al., 2019) and the larval fruit fly, *Drosophila* (Ohyama et al., 2015; Winding et al., 2022). Analysis of these datasets, combined with behavior and calcium imaging, have provided insight into motor control of peristaltic locomotion (Wen et al., 2012; Zarin et al., 2019). However, less is known about premotor circuits controlling limbed locomotion, in part because there does not yet exist a premotor connectivity map in any limbed animal.

Here, we apply connectomics to reconstruct and analyze leg and wing premotor circuits of adult *Drosophila.* The nervous system of the adult fly has about 15 times as many neurons as the larva (Winding et al., 2023; Zheng et al., 2018), but adult flies still have at least 100 times fewer MNs than limbed vertebrates like cats (Kernell, 2006). Each MN in the fly is anatomically and genetically identifiable across individuals, making it possible to systematically analyze the anatomy, physiology, and behavioral function of individual cells (Azevedo et al., 2020), including their synaptic partners within the central nervous system (**Figure 1A**) and muscle targets in the periphery (**Figure 1B**).

Flies use their six legs for many behaviors including walking, grooming, aggression, and courtship (Tuthill and Wilson, 2016). Each leg has five segments and five joints (**Figure 1C**). The position of the fly's tarsus is specified by seven mechanical degrees of freedom (three at the most proximal joint and one at each other joint (Lobato-Rios et al., 2022)). Eighteen distinct muscles actuate the leg joints, each innervated by between 1 and 10 MNs (Azevedo et al., 2022). The fly's front leg is innervated by a total of up to 70 MNs (Azevedo et al., 2022; Phelps et al., 2021). In many animals, MNs controlling the same joint typically fire in a stereotyped order, or recruitment hierarchy, to increase muscle force (Gabriel et al., 2003; Henneman et al., 1965; Hill and Cattaert, 2008; Marshall et al., 2022; McLean and Dougherty, 2015; Milner-Brown et al., 1973; Sasaki and Burrows, 1998). However, the architecture of premotor circuits that underlie the MN recruitment hierarchy have remained a mystery since the phenomenon was first observed in cats over 60 years ago (Henneman, 1957).

While motor control of the fly leg has many striking similarities to other limbed animals, several features of the flight motor system are unique to the order Diptera. In particular, flies have evolved additional flight control muscles that insert directly on sclerites, tiny thickened mechanical components within the animal's wing hinge, thus providing a capacity for motor precision that exceeds that of other insects (Hörnschemeyer, 2002; Miyan and Ewing, 1985). The fly wing motor system is also evolutionarily distinct from the leg motor system and has a unique biomechanical and neuromuscular organization. *Drosophila* beat their wings at ~220 Hz, faster than most muscles can contract while still generating sufficient power for flight. To overcome this obstacle, flies have two morphologically and physiologically distinct sets of muscles. The first set, the power muscles, span the entire thorax and power the wingstroke. As in several other groups of insects (Dudley, 2000), the neural control of the power muscles is asynchronous. Instead of a MN action potential directly triggering muscle contraction, contraction of one set of stretch-activated power muscles triggers contraction of the other set, causing the thorax to oscillate (Pringle, 1949). The second set of muscles directly control the wing for steering (Dickinson and Tu, 1997). There are no muscles within the fly wing itself, rather the 12 steering muscles reside in the thorax and attach to four sclerites within the hinge (Boettiger and Furshpan, 1952; Miyan and Ewing, 1985; Williams and Williams, 1943). Some of the steering muscles share a tendon, but others attach at different points on the same sclerite, resulting in multiple degrees of freedom for a single joint. Finally, there is also a third set of tension muscles that modify thorax stiffness (Nachtigall and Wilson, 1967; Pringle, 1957). Altogether, these flight-related muscles are innervated by 30 uniquely identifiable MNs per side (Azevedo et al., 2022; Phelps et al., 2021). Although past work has revealed mechanisms of flight motor control at the level of muscles and MNs (Balint and Dickinson, 2001; Dickinson et al., 1993; Heide, 1983, 1975; Lehmann and Bartussek, 2017; Lindsay et al., 2017; O'Sullivan et al., 2018; Whitehead et al., 2022), comparatively little is known about wing premotor circuits that control flight and other wing-related behaviors.

Leg and wing premotor circuits in the fly are both contained within the ventral nerve cord (VNC), which functions like the vertebrate spinal cord to move the limbs and process mechanosensory feedback (Court et al., 2020). In a companion paper (Azevedo et al., 2022), we applied deep learning methods for neuron segmentation and synapse prediction to an electron microscopy volume of an adult female *Drosophila* VNC (Phelps et al., 2021) (**Figure 1A**). We then combined genetic tools and x-ray tomography to determine the muscle innervation of leg and wing MNs in the connectome (**Figure 1B**). Here, we leverage those tools to reconstruct and analyze leg and wing premotor neural circuits. The existence of two biomechanically distinct locomotor systems within the same animal provides a unique opportunity to identify general and specialized properties of premotor circuit organization.

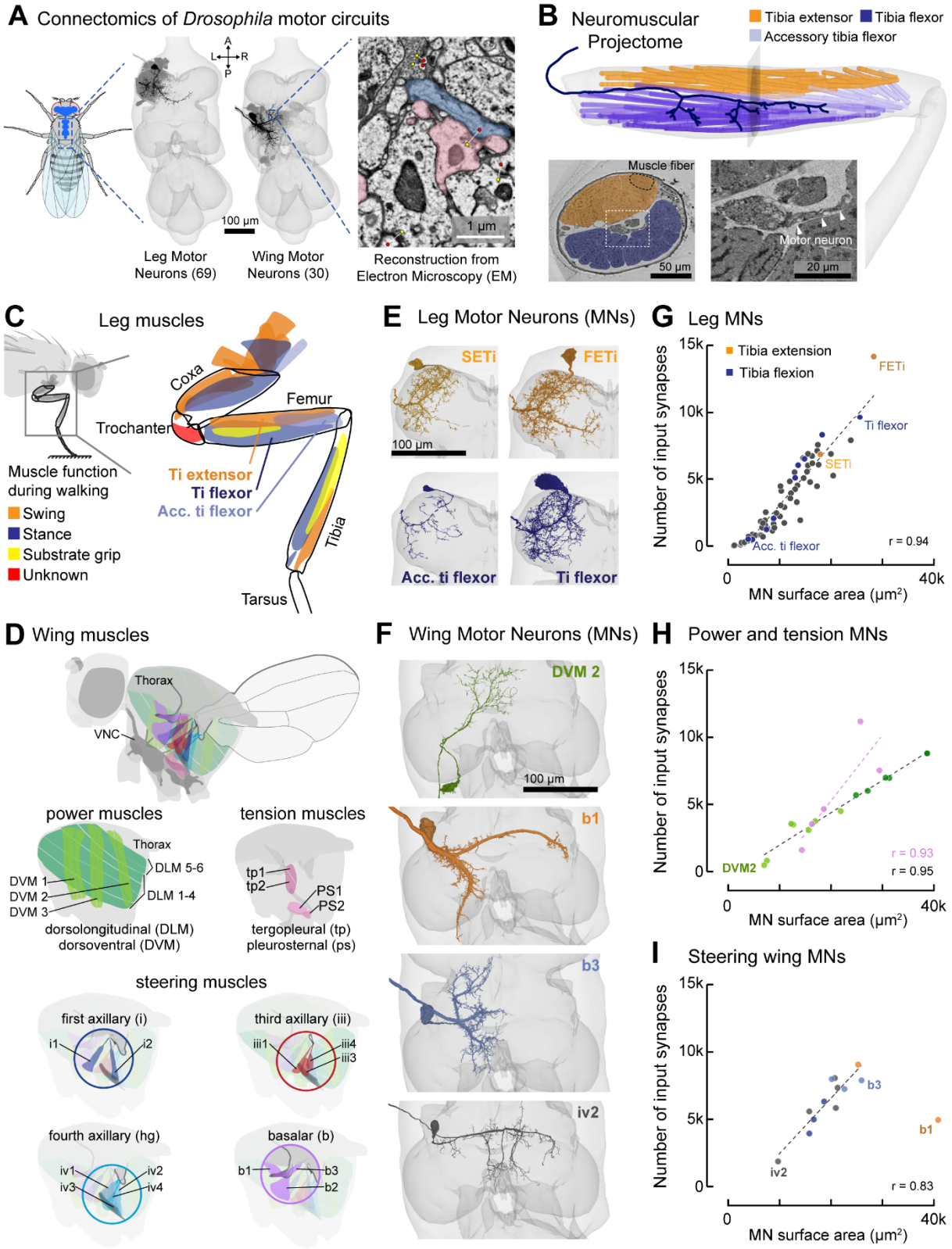

Figure 1. Reconstruction of synaptic inputs to identified leg and wing MNs in *Drosophila*. (**A**) Automated neuron segmentation and synapse prediction in a serial-section electron microscopy volume of an adult female VNC. The VNC contains the MNs for controlling the leg (left, N = 69 MNs) and the wing (right, N = 30 MNs). Predicted synapses are marked in the EM image: yellow dots denote presynaptic sites; red dots denote postsynaptic sites. (**B**) The muscle innervation pattern of each MN was determined by combining EM reconstruction with x-ray tomography of the leg (bottom panels) and genetic driver lines (Azevedo et al., 2022). (**C**) Schematic of the 18 muscles controlling the front leg. (**D**) Flight musculature, separated according to muscle physiology and/or tendon insertion anatomy. (**E**) Reconstructed MNs that extend and flex the tibia. (**F**) Reconstructed wing MNs. (**G**) Leg MN input synapses scale linearly with MN surface area ($r=0.95$, $p<10^{-34}$, slope of 0.34 synapses/µm^2). (**H**) MN input synapses vs. MN surface area for DLM MNs (dark green) and DVM MNs (light green, slope=0.15 synapses/µm^2, $r=0.95$, $p<10^{-5}$), and for tension MNs (slope=0.38 synapses/µm^2, $r=0.91$, $p=0.01$). (**I**) MN input synapses vs. MN surface area for wing steering MNs (slope=0.21, $r=0.83$, $p<10^{-3}$, excluding the enormous b1 neuron).

Results

Using software for collaborative proofreading and visualization of the segmented EM dataset (see **Methods**), we reconstructed the anatomy and synaptic connectivity of all premotor neurons (preMNs) that synapse onto motor neurons (MNs) controlling a fly leg and wing. The resulting leg premotor connectome consists of 69 MNs that receive 220,747 synapses from 1,411 preMNs, whereas the wing premotor connectome consists of 30 wing and thorax MNs that receive 151,030 synapses from 1,787 preMNs. MNs have tortuous dendritic arbors and are among the largest cell bodies in the *Drosophila* nervous system (**Figure 1E-F**). On average, each MN receives 3,883 input synapses from 256 preMNs and each preMN synapses onto 5 MNs (using a 3 synapse threshold; **Extended Data Figure 1**).

In all limbed animals studied to date, including insects, MN soma size is correlated with the number and physiology of the muscle fibers within its motor unit and with the amount of force the motor unit produces (Burrows, 1996; Cullheim, 1978; Hill and Cattaert, 2008; Hoyle, 1983; Kernell, 2006; Mcphedran et al., 1965; Monster and Chan, 1977; Wuerker et al., 1965). Unlike in vertebrates, the soma of insect MNs do not typically receive synaptic input and thus do not serve an important role in neural processing. Nonetheless, when we measured the volume and surface area of leg and wing MNs, not including the portions beyond which their axons were cut in the nerve, we found that leg and wing MN size varied significantly, even for MNs controlling the same joint (**Extended Data Figure 1**). This variation in MN size is consistent with prior work in other species (Cullheim et al., 1987; Kernell and Zwaagstra, 1989). However, it has not previously been possible to determine how MN size is related to the number of synapses it receives from preMNs.

For leg MNs, we found that the total number of input synapses is highly correlated with MN surface area ($r=0.94$, $p<10^{-33}$); larger leg MNs receive more synapses, with a slope of 0.45 synapses/μm^2 (**Figure 1G**). This is approximately 3X more synapses per unit area than reported for vertebrate MNs (Örnung et al., 1998). MNs that innervate wing power muscles also feature a correlated gradient between synapse number and MN surface area (slope=0.24 synapses/μm^2, $r=0.98$, $p<10^{-7}$), as do tension MNs (slope=0.49 synapses/μm^2, $r=0.84$, $p=0.07$) (**Figure 1H**) and steering MNs, so long as the b1 MN is excluded (slope=0.21, $r=0.83$, $p<10^{-3}$) (**Figure 1D, I**). Thus, we observed consistent correlations between cellular size and synaptic input strength across both leg and wing MNs.

Local neurons make up the majority of the premotor connectome for both walking and flight.

Motor neurons receive synaptic input from several different classes of premotor neurons (preMNs), including local interneurons and descending neurons from the brain. Apart from *C. elegans* and larval *Drosophila* (Cook et al., 2019; Winding et al., 2022; Zarin et al., 2019), both crawling animals, it has not previously been possible to measure the proportion of synaptic input from different preMN classes. To compare sources of premotor synaptic input to leg and wing MNs, we classified preMNs into five morphological classes: descending, sensory, ascending, intersegmental, and local neurons (**Figure 2A-C**, see **Methods**). We then plotted the full connectivity matrices of all preMNs (rows) onto MNs (columns), sorted according to the preMN class we defined (**Figure 2D-E**). We found that the predominant source (~60%) of synaptic input to both leg and wing MNs is from local VNC neurons (**Figure 2D-F, Extended Data Figure 1**). Leg and wing MNs integrate similar proportions of descending input from the brain (~10%), and intersegmental input from other VNC segments (~15%). They also both receive ~3% of their synapses from sensory neurons, similar to the estimate of sensory afferent input to MNs in vertebrates (Burke and Glenn, 1996). Previous work in the fly has focused on the contributions of descending neurons to fly motor control (Bidaye et al., 2014; Feng et al., 2020; Namiki et al., 2018; Schnell et al., 2017). However, the composition of the leg and wing premotor connectomes reveals that local VNC preMNs play a dominant role in direct premotor control.

Common preMN input groups MNs into motor modules with gradients in MN size.

We next asked whether preMN connectivity reflects the function of the muscles innervated by each MN. We sorted the MNs (columns) of the two connectivity matrices according to their muscle targets (**Figure 2D-E**). The vertical stripes in both the leg and wing connectivity matrices (**Figure 2D-E**) indicate that preMNs tend to synapse onto MNs with similar function.

To quantify this structure, we calculated the cosine similarity score for pairs of MNs based on their synaptic input from preMNs (**Figure 3A**). Two MNs are similar if they receive the same input weights from the same preMNs (i.e. the same relative number of synapses, relative to total input). Low similarity scores indicate either that two MNs share few synaptic partners or that the relative input weights from common preMNs are different.

We found that leg MNs that innervate related muscles receive similar preMN input, and thus cluster together within the pairwise similarity matrices (**Figure 3B**). Within some clusters, the similarity scores were as high as 0.96. We refer to these MN clusters as modules, and found evidence for them in both the leg and wing motor systems. Most leg MNs (53 out of 69) belong to modules with

MNs that target two or more muscles that control the same joint (**Figure 3B**). For instance, the Tibia Flex A module includes five MNs that target the main tibia flexor muscle, along with four of the ten MNs that innervate the separate accessory tibia flexor muscle. The accessory tibia flexor is an example of a muscle that is innervated by MNs from three separate modules; five other accessory tibia flexor MNs cluster in an additional module (Tibia Flex B), and the tenth MN forms a separate module altogether (Tibia Flex C). This organization is similar to that of tibia flexor MNs in locusts (Hoyle, 1955; Sasaki and Burrows, 1998). On the other hand, MNs that innervate muscles that control the tarsus receive little common input with each other and instead separate out into the three

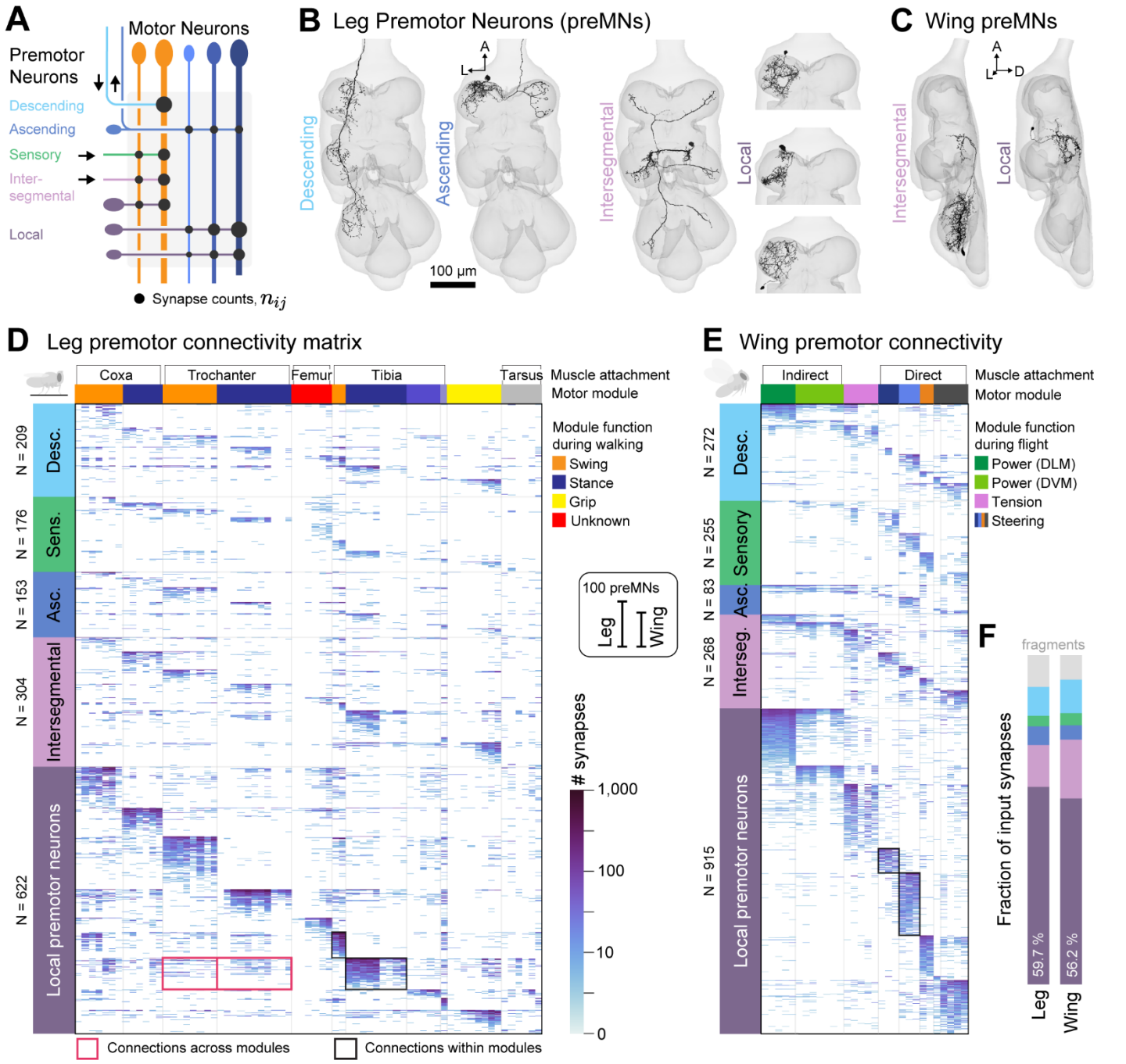

Figure 2. The majority of synaptic input to MNs is from local premotor neurons (preMNs). (**A**) Schematized premotor connectivity matrix. PreMNs are colored according to cell class. MNs are represented vertically and grouped into modules (orange and blue) based on shared preMNs. (**B**) Example descending, ascending, intersegmental, and local leg preMNs. Intersegmental leg preMNs receive input from outside of the neuromere. (**C**) Example intersegmental and local wing preMNs. Intersegmental wing preMNs receive input from leg neuromeres. (**D**) Premotor connectivity matrix for the left T1 leg. The color of each tick indicates the log10(n_{ij}+1) of the number of synapses from each preMN, i (row) onto each MN, j (column). Note, the logarithm makes differences appear smaller than they are. MNs are ordered according to muscle target, from proximal to distal, grouped into modules indicated with gray vertical lines and colors (top). PreMNs are ordered: 1) by cell class; 2) by preferred motor module (see **Methods**); 3) by total synapses onto all MNs. (**E**) Same as E, for wing MNs. Wing MNs (N=30) are grouped by similarity of premotor inputs (see **Methods**). (**F**) Fraction of total synaptic input from each cell class onto leg or wing MNs. The majority of synaptic premotor input comes from interneurons intrinsic to the VNC (local and intersegmental).

tibia flexion modules. For example, the Tibia Flex A module also includes a single tarsus MN. Premotor input to the tibia flexion modules would thus co-contract the tarsus and tibia muscles to synergistically actuate the pair of linked joints.

In the wing motor system, power and steering are controlled by entirely different muscle groups. This distinction was clearly reflected in the premotor connectome by the separate clustering of power, tension, and steering MNs (**Figure 3C**). MNs that innervate the power muscles clustered into two modules according to the orientation of the muscles they innervate. The MNs that innervate dorsolongitudinal muscles (DLMs) and dorsoventromedial muscles (DVMs) receive a high degree of common input within each muscle group (similarity=0.94 and 0.82), as well as common input with each other (similarity=0.5), but little common input with tension or steering MNs (similarity=0.05).

The twelve MNs innervating steering muscles formed four distinct clusters in the similarity matrix (**Figure 3C**), which we refer to as Steering Modules A-D. Unlike the leg, these wing steering modules contained MNs that innervate muscles with different attachment points (**Figure 3D**), although their mechanical functions may be similar. Prior analysis of wing hinge anatomy (Miyan and Ewing, 1985), electrophysiology (Heide, 1983) and calcium imaging from steering muscles in flying flies (Lindsay et al., 2017) allow us to predict specific functions for each of these modules (see **Methods**).

Steering module A is made up of one tension MN (tpn) and two MNs that attach to the same sclerite (third axillary, iii). We predict that this module is involved with wing extension, as well as increasing wingbeat amplitude. Steering module B is made up of two MNs that attach to the first sclerite (i1 and i2), as well as one MN that attaches to the basalar sclerite (MN b3), and we predict that these muscles are used to decrease wingbeat amplitude, especially in the case of ipsilateral turns. Steering module C contains MNs that innervate the other two basalar muscles (b1 and b2), which are antagonistic to b3. These muscles are the most well characterized in prior research (Heide, 1983; Tu and Dickinson, 1996; Whitehead et al., 2022), and we predict that this module is necessary for pitch stabilization and the constant adjustment of wingbeat amplitude. Finally, Module D is the most perplexing, as it contains MNs that innervate muscles of the fourth axillary sclerite (iv1, iv2, iv3, and iv4), which are thought to be organized into two antagonistic groups based on their insertion pattern (Miyan and Ewing, 1985; Williams and Williams, 1943), as well as a small muscle (iii4) that attaches to the third axillary. However, we do not propose a function for this module due to the fact that few electrophysiological recordings exist from these muscles in any fly species, due to their small size. Another important caveat to these predictions is that prior work measured muscle activity or sclerite movement in either tethered or dead flies, which may be significantly different than under free-flight conditions (Fry et al., 2003; Muijres et al., 2014). Furthermore, we considered wing motor modules primarily in the context of flight, but flies also move their wings during grooming and courtship (Shiozaki et al., 2022; Zhang and Simpson, 2022), although less is known about steering muscle activity during these behaviors.

In summary, we find leg and wing premotor networks have distinct modular structure. For the leg, MNs that innervate adjacent muscles with synergistic functions cluster together into modules that receive similar patterns of synaptic input from preMNs. In the wing, MNs that innervate muscles for powering the wingstroke, steering, or adjusting thorax tension cluster independently. Steering MNs are then further subdivided into modules that likely control specific aspects of wingstroke kinematics. Next, we consider how preMNs distribute their synaptic input within and across modules.

PreMNs preferentially synapse onto specific motor modules.

The leg and wing connectivity matrices (**Figure 2D-E**) show that preMNs tend to synapse onto MNs within a module and to make fewer synapses onto other modules. To quantify these patterns, we computed the "module preference" of each preMN, defined as the sum of synapses onto all MNs in a single module divided by the sum of synapses onto all MNs. We found that most preMNs, of all classes, make the majority of their synapses onto MNs in a single module (module preference > 0.5) (**Figure 3E, Extended Data Figure 2**). Intuitively, one might assume that high module preference for preMNs should lead to high similarity among MNs within the module. However, cosine similarity depends on the relative input weights from each preMN (**Figure 3A**), so MNs that receive common preMN input do not necessarily have high cosine similarity. Indeed, intersegmental and descending preMNs have higher median module preference than local preMNs, yet measuring MN similarity based on those connections alone resulted in lower within-module similarity scores (**Figure 3F**, **Extended Data Figure 2**). We observed a similar trend for tension and steering MNs in the wing motor system, where preMNs showed high module preference yet MN similarity was consistently lower than leg similarity. The mismatch between high module preference and low similarity in wing modules suggests a fundamental difference in how local preMNs synapse onto MNs preferred modules. Therefore, we set out to quantify the synaptic connectivity that gives rise to this observation in order to understand its implications for motor control.

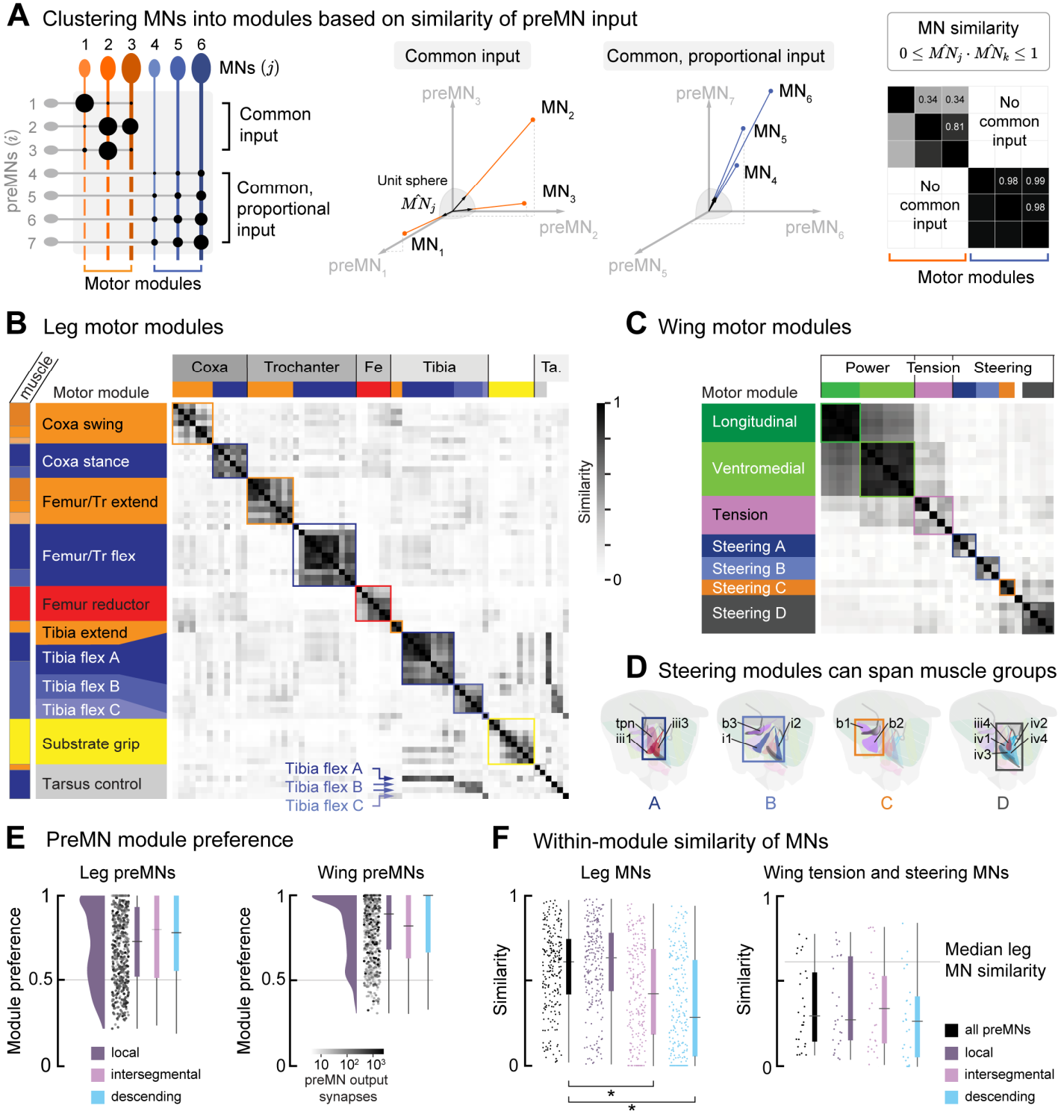

Figure 3. PreMNs preferentially target groups of MNs, forming motor modules. (**A**) Hypothetical connectivity patterns illustrate quantification of MN similarity. MN similarity is the dot product of the normalized (unit) column weight vectors, $\widehat{MN}_j$. If two MNs receive the same synaptic weights from the same preMNs (blue), relative to the total input, the pairwise similarity is 1. For MNs that receive shared input with non-proportional weights (orange), the unit vectors point in different directions with low pairwise similarity. (**B**) Pairwise MN similarity matrix for leg MNs. MNs are ordered as in **Figure 1**, from proximal muscle targets to distal. Muscle innervation of each MN is indicated in the leftmost column (Azevedo et al., 2022). Motor modules, based on clustering of similarity scores (see **Methods**), are indicated to the right and at top. (**C**) Pairwise similarity of wing MNs. Wing MNs are ordered by motor module (see **Methods**). (**D**) Steering modules are composed of motor units that control distinct sclerites. (**E**) Module preference for local (purple), intersegmental (pink), and descending (blue) leg preMNs, the three cell classes that account for the majority of MN input. Module preference is defined as the (sum of the number of synapses onto each MNs in a module) / (total number of synapses onto all MNs). Dots represent individual local preMNs, with grayscale indicating the total number of synapses on a log scale. Left, leg preMNs. Right, wing preMNs. (**F**) Pairwise similarity of MNs within modules, when considering all preMNs (black), or just a single class. Left: within-module leg MN similarity is lower when considering only intersegmental or descending preMNs ($p<10^{-24}$, Kruskal-Wallis non-parametric one-way ANOVA. Conover's post-hoc pairwise test with Holm correction for multiple comparisons: * - $p<10^{-6}$). Right: within-module similarity of wing MNs (excluding power MNs) is generally lower than for leg MNs. The power modules exhibit stronger within-module similarity (**Extended Data Figure 3**).

The structure of common input to leg and wing motor modules reflects their biomechanical function.

A previous study used electrophysiology in behaving flies to measure recruitment patterns of leg MNs (Azevedo et al., 2020). This analysis showed that tibia flexor MNs fire in a hierarchical order that is correlated with their size, excitability, and neuromuscular gain, consistent with Henneman's size principle (**Figure 4A**). Our finding that leg MNs cluster into modules based on preMN input similarity (**Figure 3B**) is consistent with recruitment hierarchy models based on the size principle, which assume that MNs within a module share common premotor input. This assumption was based on the one-to-all connectivity of muscle spindle 1a afferents in the vertebrate spinal cord (Burke and Glenn, 1996; Mendell and Henneman, 1971; Scheibel and Schiebel, 1969), and supported by measured correlations in MN firing rates (De Luca and Erim, 1994; Hug et al., 2023). According to the size principle model, the gradient in MN excitability dictates the order in which MNs reach spike threshold in response to common synaptic input (Henneman et al., 1965).

By comparison, the lower within-module similarity of wing steering MNs (**Figure 3F**) suggests that the wing motor system employs a distinct recruitment scheme. Compared to leg joints, which typically have only 1-2 degrees of freedom (**Figure 4B**), the fly wing hinge is an intricate structure with many degrees of freedom, although its biomechanical operation during flight is not yet fully understood (Deora et al., 2017). MNs within each wing steering module attach to different wing hinge sclerites, and thus exert different mechanical effects on the wing hinge (**Figure 4C**). However, each of the four sclerite groups appear to contain at least one tonically active muscle, which continuously tunes the motion of the wing, and one phasically active muscle, that is typically recruited in bursts during maneuvers (Lindsay et al., 2017). Prior electrophysiological (Balint and Dickinson, 2001; Heide and Götz, 1996; Tu and Dickinson, 1996) and biomechanical (Tu and Dickinson, 1994) studies suggest that the action of both the tonic and phasic muscle MNs are regulated by firing phase within the wingbeat cycle, and provide the flight circuitry with a means of adjusting wing motion with high precision despite the small number of motor units involved. If each steering muscle has unique effects on the wing's trajectory, and these effects depend on the phase of firing within the wingstroke, then it could be advantageous for preMNs to recruit wing steering MNs in different combinations and sequences, rather than simply following a hierarchical recruitment order. Thus, we speculate that the connectivity within wing steering modules may be less orderly than leg modules. This would explain why the within-module similarity scores for wing steering modules are lower than for leg modules (**Figure 3F**), despite similarly high levels of module preference (**Figure 3E**).

We first analyzed the structure of local preMN input to leg motor modules controlling the tibia. We quantified the structure of local preMN synaptic input onto MNs in their preferred module (module connectivity, **Figure 4D**). We defined the output weight, w_{ij}, as the synapse count from preMN, i, onto MN, j, divided by the sum of the synapses onto the entire motor module (**Figure 4D**). We found that each preMN provides the same output weight onto all the MNs within the extensor (**Figure 4E**) and flexor modules (**Figure 4F**). Specifically, the preMN output weights onto each MN are proportional to the overall synaptic input to each MN. This is true regardless of total preMN synapses, which can range over 100-fold (**Figure 4E-F**). This pattern of proportional weights is a key determinant of MN input similarity (**Extended Data Figure 3**).

When we performed a similar analysis on wing steering modules, we found an entirely different organization. In contrast to the consistently proportional synaptic weights across leg modules, wing Steering Modules A and B exhibit non-proportional weights from local preMNs (**Figure 4G-H**). We propose that this organization provides an anatomical basis for recruiting MNs in different combinations and sequences depending on behavioral context. For example, the wing is extended to open the wings to initiate flight as well as to move the wing through the wingbeat cycle. These movements may recruit the same muscles but in different orders within each behavioral context.

Steering Module C, which contains only two MNs, is characterized by inversely proportional weights, such that the smaller b2 MN receives a greater proportion of input from most common local preMNs (**Figure 4I-J**). A possible reason for this difference is the demand for temporally precise b1 MN activation during flight. Increasing the diameter of a neuron's axon increases the conduction velocity of action potentials. Conduction velocity may be particularly critical for the b1 MN, as it fires an action potential on every wingstroke (~220 Hz) and is necessary for maintaining wingstroke amplitude (Heide, 1983; Tu and Dickinson, 1996). Further, the phase within the wingstroke at which the b1 MN spike arrives has been shown to regulate the stiffness of its target muscle and thus its effect on wing kinematics (Tu and Dickinson, 1993).

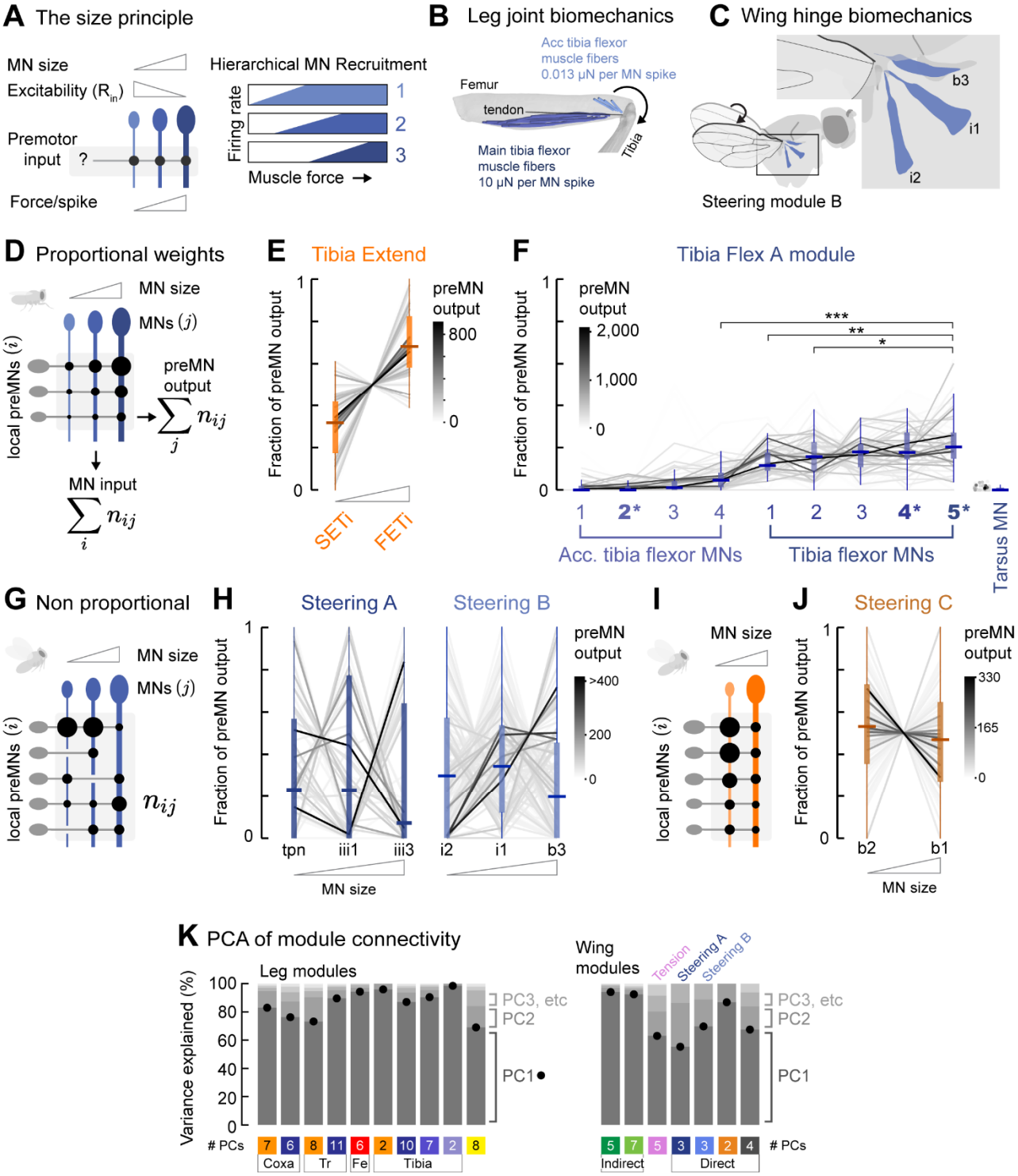

Figure 4. Local preMN connectivity differs between leg and wing steering motor modules. (**A**) The size principle for hierarchical MN recruitment. MNs that receive common premotor input are recruited in order from smallest to largest due to a gradient in excitability. Increasing common drive recruits larger MNs with higher neuromuscular gain. (**B**) Force produced at the tip of the tibia by two motor units in the Tibia Flex A module (Azevedo et al., 2020). (**C**) Schematic of muscle attachment for the WBA Decrease steering muscles. Each muscle has a different origin and attachment to the wing hinge. (**D**) Leg modules exhibit proportional connectivity. PreMN output is defined as the sum of each preMN's synapses onto MNs in the module. (**E**) Proportional connection weights from local preMNs onto the Slow (SETi) and Fast (FETi) tibia extensor MNs. Line grayscale indicates preMN output. (**F**) Proportional connection weights from local preMNs onto the Tibia Flex A module. The module is composed of four accessory tibia flexor MNs, the five main tibia flexor MNs, and the synergist tarsus MN. Tibia MNs are ordered by volume. Asterisks indicate MNs previously characterized using electrophysiology. The muscle fiber targets of 2* and 5* are shown in (**B**) (Azevedo et al., 2022, 2020). The fraction of preMN output onto the largest MN is significantly larger than onto smaller MNs ($p<10^{-4}$, Kruskal-Wallis non-parametric one-way ANOVA. Conover's post-hoc pairwise test with Holm correction for multiple comparisons: *** - $p<10^{-28}$, ** - $p<10^{-4}$, * - p=0.012). (**G**) Wing steering motor modules lack proportional connectivity. (**H**) Local preMN connections onto wing Steering Modules A and B. (**I**) Schematic of module connectivity for Steering Module C. PreMNs make more synapses onto the smaller b2 MN than the larger b1 MN. (**J**) Same as (**E**) for Steering Module C. (**K**) Principal Components Analysis of the connections between local preMNs and their preferred motor module. Dots and dark gray bars indicate the percent of the module connectivity variance that is explained by a single principal component, for each leg and wing module.

To quantify these properties of within-module connectivity across all leg and wing modules, we performed principal component analysis (PCA) on the connectivity matrix of each motor module (**Figure 4K**). We found that the first principal component was sufficient to explain the majority (>80%) of the variance within most leg motor modules. The percentages of variance explained within modules for the wing power MNs were also high (>90%). For both leg modules and the modules of the wing power muscles, the only significant dimension of variation (captured by the first component alone) was simply the overall preMN output onto the modules (**Figure 4K, Extended Data Figure 4**). However, the first principal component explained a lower fraction of the variance for modules controlling the wing steering muscles. This incongruity suggests that the second and third components are unlikely to reflect noise, but rather represent distinct pathways for alternate MN recruitment orders.

In summary, the strength of preMN input to leg motor modules is proportional to total MN input, while premotor input to wing motor modules associated with the steering muscles is not. This difference explains why modules controlling the wing steering muscles have lower within-module similarity then leg modules (**Figure 3E**). Uneven patterns of preMN connectivity may allow wing steering MNs to be recruited in different combinations, or with different relative timing. Fine-scale control of the order and timing of MN activation may be more important for wing steering because the muscles attach to different sclerites and thus have distinct biomechanical effects on the wing. In support of this interpretation, the leg modules with the least proportional module connectivity (**Figure 4K**) include leg MNs that innervate biarticular muscles, i.e. muscles and tendons that originate on one structure, cross two joints, and then insert on the next structure (**Extended Data Figure 4**). Biarticular muscles have distinct effects on leg dynamics compared to their monoarticular counterparts, perhaps necessitating more diverse preMN connectivity patterns (Graham and Scott, 2003; Lillicrap and Scott, 2013).

We propose that the connectivity of wing preMNs provides a basis for tuning the recruitment order of MNs within a module, whereas the connectivity of leg preMNs provides a basis for fine-scale control of joint force production (**Figure 4B**). Patterns of proportional connectivity support the hypothesis that common premotor input underlies recruitment hierarchies within each leg module. The precision of proportional preMN connectivity onto leg MNs is striking, especially considering the lack of spatial topography among MNs within the leg neuropil of the fly VNC (Azevedo et al., 2022). During development, each preMN must somehow find its target module and establish the appropriate number of synapses onto each MN, according to MN size (**Extended Data Figure 3**) (Mendell and Henneman, 1971). To shed light on this question, we next analyze how the structure of synaptic connectivity within each motor module is related to preMN developmental origin.

Excitatory local preMNs make more synapses onto non-preferred motor modules.

In *Drosophila*, neurons that share a developmental origin possess common anatomical features (Truman et al., 2004) and release the same neurotransmitter (Lacin et al., 2019). About 95% of adult VNC neurons in each segment develop from sets of 30 paired and one unpaired neuroblast (Shepherd et al., 2019). Neuroblasts in each VNC segment repeatedly divide to form neuronal hemilineages (**Figure 5A**). Thermogenetic activation of individual VNC hemilineages can drive coordinated movements of the legs or wings (Harris et al., 2015), suggesting that developmentally related cells may form functional motor circuit motifs. Consistent with these findings, we found that some hemilineages contain preMNs that predominantly synapse on either leg or wing MNs (**Figure 5B**). However, preMNs within a hemilineage always target multiple motor modules within the leg or wing networks. Each module also receives synaptic input from preMNs from multiple different hemilineages. Thus, preference of preMNs for a particular module is not strictly linked to their developmental origin.

The majority of *Drosophila* neurons release one of three primary neurotransmitters (Allen et al., 2020; Li et al., 2022): acetylcholine (which is typically excitatory), GABA (typically inhibitory), or glutamate (typically inhibitory). Based on morphology, we determined the neurotransmitter identity of ~80% of the local and intersegmental preMNs (**Extended Data Figure 5**). Both leg and wing MNs receive a remarkably consistent ratio of excitatory and inhibitory synapses (average E/I ratio of 0.99±0.72 std, **Figure 5C**). This balance of excitation and inhibition appears to be tightly regulated, as it is similar across MNs that differ up to 40-fold in size and total synaptic input.

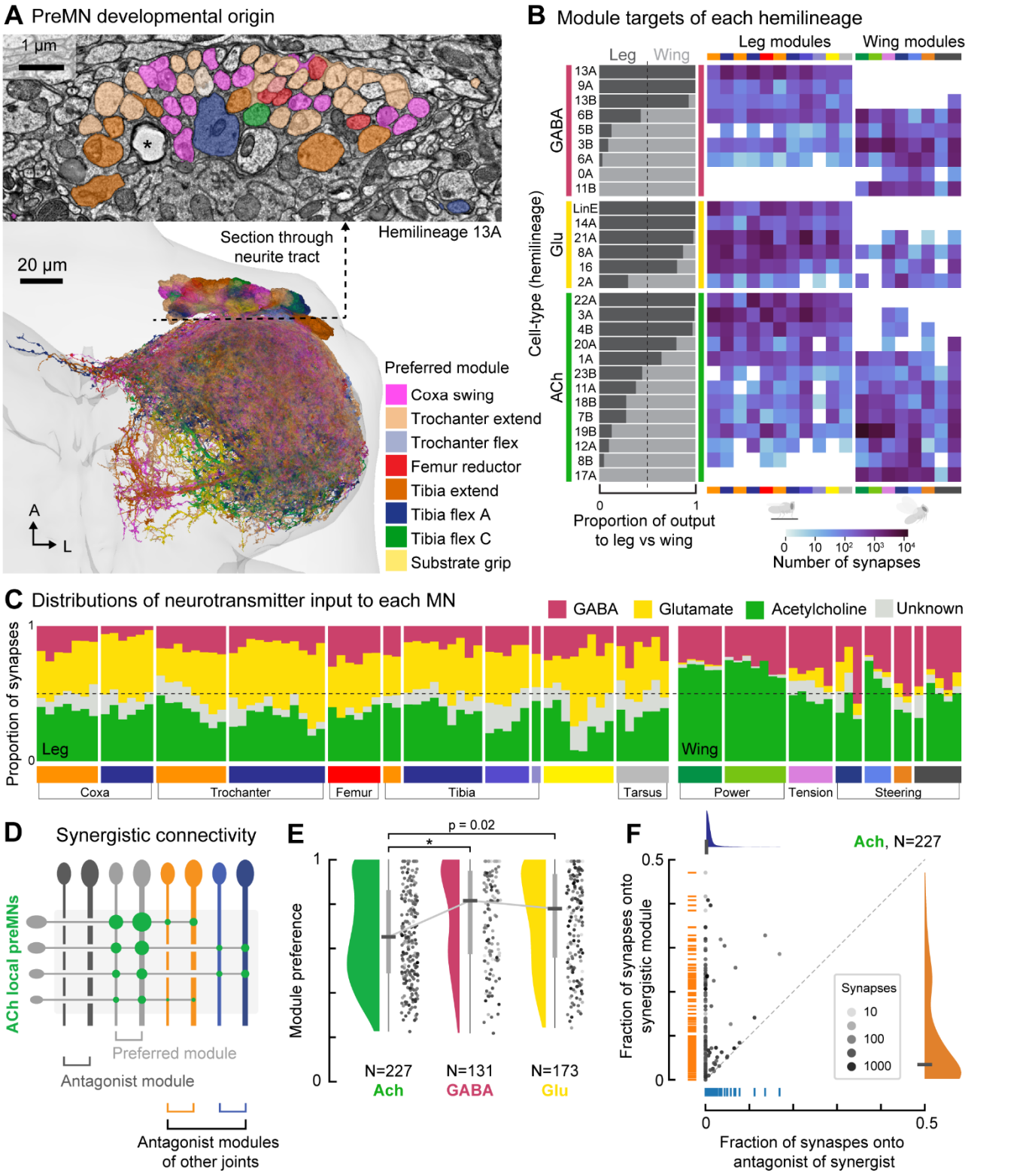

Figure 5. Hemilineage identification reveals that all MNs receive balanced excitatory/inhibitory synapses. (**A**) PreMNs within a hemilineage are anatomically diverse. Example shows individual preMNs from hemilineage 13A (GABAergic), colored according to their preferred leg motor module. (**B**) Left: proportion of the total synapses from all local and intersegmental preMNs in each hemilineage onto leg MNs vs. wing MNs. Right: total synapses onto MNs in each leg or wing module. (**C**) Proportion of synaptic input to MNs from cholinergic (green), glutamatergic (yellow), GABAergic (pink), and unidentified (light gray), hemilineages. Only local and intersegmental preMNs are included in this analysis (see Methods). (**D**) Cholinergic preMNs target leg modules other than their preferred modules, but avoid synapsing onto antagonist modules. (**E**) Module preference score for local leg preMNs, classified by hemilineage neurotransmitter. Dot grayscale indicates total synapses onto all MNs, same scale as (F). (p=0.0013,, Kruskal-Wallis non-parametric one-way ANOVA. Conover's post-hoc pairwise test with Holm correction for multiple comparisons: * - p=0.002). (**F**) Relative fraction of output synapses from cholinergic preMNs onto antagonist modules other than the preferred module. The "synergist module" is the module with the largest fraction of total preMN synapses, after the preferred module (y-axis). The x-axis is the fraction of total preMN synapses onto the antagonist of the synergist module. Dot grayscale indicates total synapses onto all MNs.

Finally, we examined whether the connectivity patterns of local leg preMNs depend on neurotransmitter identity (**Figure 5D)**. As we saw above (**Figure 4**), all local leg preMNs, including both inhibitory and excitatory neurons, tend to make proportional weights onto their preferred module. However, the module preference is lower for excitatory preMNs than for inhibitory preMNs (**Figure 5E)**, indicating that excitatory preMNs tend to make fewer synapses within a module and more synapses onto other modules. Local preMNs rarely synapse onto the antagonist of their preferred module (**Figure 5D**). For example, the leg connectivity matrix (**Figure 2D**) shows that local preMNs that prefer the Tibia Flex A module generally do not synapse on MNs within the Tibia Extend module. This means that excitatory leg preMNs tend to synapse onto modules that control other joints. Furthermore, when an excitatory preMN synapses on multiple modules, it also avoids synapsing onto the antagonist of the second module (**Figure 5F**). For instance, if an excitatory preMN preferentially synapses on MNs in the Tibia Flex A module, and also synapses onto trochanter flexor MNs (synergist), then it does not synapse onto trochanter extensor MNs (antagonist of the synergist). Thus, while all leg preMNs have stereotyped synaptic weights within their preferred leg modules (**Figure 4DE-F**), excitatory preMNs are distinguished by their precise patterns of cross-module connectivity (**Figure 5E-F**).

Discussion

We took advantage of the tractable scale of the *Drosophila* nervous system to comprehensively reconstruct the synaptic organization of premotor circuits controlling the movement of the legs and wings. Because comparison is essential for identifying principles of neural circuit organization, we chose to analyze these two unique premotor networks side by side. Our analysis revealed striking similarities and fundamental differences between the two motor systems. We propose that the similarities represent general solutions to the challenge of limb motor control. The differences likely reflect contrasting demands for smoothly controlling torque at leg joints vs. altering the wingstroke trajectory through transient forces acting on different parts of the wing hinge. As the first analysis of a premotor connectome in a limbed animal, our results provide a conceptual foundation and clear hypotheses that motivate reconstruction of premotor networks in other animals with diverse modes of locomotion.

Similarities between wing and leg premotor networks

A typical *Drosophila* MN receives thousands of synapses from hundreds of presynaptic preMNs (**Figure 3D-E, Extended Data Figure 1**). This proportion is on par with the scale of synaptic integration in pyramidal cells of the rodent cortex (Schneider-Mizell et al., 2023), but ten times fewer synapses than cat MNs (16,000 - 140,000; (Kernell and Zwaagstra, 1989; Örnung et al., 1998; Ulfhake and Cullheim, 1988). Both leg and wing MNs in the fly receive the majority (>70%) of their synaptic input from preMNs intrinsic to the VNC. A small fraction of the synaptic input to MNs (<10%) is from 481 descending neurons (out of ~500 total bilateral pairs, (Namiki et al., 2018)). The massive input from local and intersegmental VNC neurons is likely responsible for low-level sensorimotor control, including the implementation of task-related descending commands (Atwood and Wiersma, 1967; Todorov et al., 2005).

Comparing the sources of presynaptic input revealed clusters of MNs that share common connectivity patterns, forming motor modules. For both leg and wing motor modules, preMNs tend to provide common input to MNs within the same module (**Figure 3**). We also found that input from local and intersegmental interneurons is made up of a balanced ratio (~1:1) of excitatory to inhibitory synapses, which is consistent across leg and wing MNs, regardless of module connectivity (**Figure 5**). This is a slightly higher ratio than for cat MNs, where inhibitory synapses outnumber excitatory synapses by ~3:2 (Örnung et al., 1998).

The balance of excitatory and inhibitory input to each module is provided by preMNs from diverse developmental origins. Regardless of their developmental identity, most preMNs preferentially synapse within one specific motor module (**Figure 3**). A similar organization has been described for the motor networks that control crawling in the *Drosophila* larvae (Mark et al., 2021). A potential mechanism for preMN target precision is the stereotyped dendritic morphology of MNs with the same muscle targets, which allows sequentially born preMNs to find postsynaptic MNs with similar morphology (Azevedo et al., 2022; Baek and Mann, 2009; Brierley et al., 2012; Enriquez et al., 2015; Guan et al., 2022). In larval zebrafish, MN birth order also determines which motor pool a preMN targets (McLean and Fetcho, 2009). In the mammalian spinal cord, preMNs preferentially connect to either flexor or extensor pools (Kiehn, 2016), but flexion and extension preMNs are spatially intermingled (Ronzano et al., 2022). In the fly, the dendrites of MNs in different motor modules are also highly intermingled within the neuropil (Azevedo et al., 2022; Balaskas et al., 2019). This lack of spatial topography means that it would not have been possible to understand the structure of premotor networks without the use of connectomics to comprehensively map patterns of premotor synaptic connectivity. This is likely to be true in the spinal cord as well.

Differences between wing and leg premotor networks

Unlike other flying animals, like birds, bats, and pterosaurs, insect wings evolved *de novo*, without repurposing a set of legs used for walking (Dudley, 2002; Kukalova-Peck, 1978). The fly therefore provides a unique opportunity to compare how neural circuits support or reflect distinct biomechanical needs within a single animal. We used what was previously known about *Drosophila* biomechanics to guide our exploration of the connectome underlying distinct movements. The *Drosophila* wing has separate muscle groups for powering the wingstroke and for steering (Dickinson and Tu, 1997; Williams and Williams, 1943). Consistent with this anatomical and physiological separation, our analysis of the premotor connectome revealed discrete motor modules for powering the flight motor and adjusting the wingstroke. The structure of the modules controlling the power muscles resemble those of the leg motor system; the number of input synapses scales proportionally with MN size. The modules controlling the wing steering muscles, however, feature non-proportional patterns of connectivity of preMNs onto MNs. Each module of the wing steering system contains muscles with distinct mechanical functions, some of which were not previously predicted to receive common input. How each muscle within a module alters the wing hinge to modify the wingstroke is unclear, as are the developmental mechanisms that give rise to such complex synaptic patterns. Diverse patterns of within-module connectivity may support a wide space of possible MN and muscle activity patterns that are needed to fine-tune wingstroke amplitude and timing.

For well-studied leg modules that flex and extend the tibia (**Figure 4D-F**), the wiring of the leg premotor input supports the prediction from the size principle that common excitatory input hierarchically recruits MNs to fire in a particular order (Azevedo et al., 2020; Burrows, 1996; Newland and Kondoh, 1997; Sasaki and Burrows, 1998). However, the size principle model does not specify the scale or structure of common input (De Luca and Erim, 1994). We discovered that common input to each motor module is in fact composed of many preMNs (~60), both excitatory and inhibitory (**Figure 5**). Each preMN connects to its preferred module in a consistent manner, regardless of which other modules it contacts or how many total synapses it makes onto MNs (**Figure 4**). Namely, the proportion of synapses a preMN makes onto an MN within its preferred module scales linearly with the size of the target MN. This synaptic weight gradient highlights the need for a reciprocal gradient in excitability to ensure that leg MNs are recruited in the correct order. Patterns of voltage- and ligand-gated ion channel expression likely complement the electrotonic properties of MN morphology to create non-linear excitable membranes that enforce the rank order of recruitment (Binder et al., 2020, 1983). Overall, the structure of synaptic connectivity within leg modules means that individual preMNs excite or inhibit all the MNs within its target leg module, and that activity of MNs within a module are collectively modulated by changes in preMN firing rate.

Subverting the recruitment hierarchy

Although MNs within a pool typically fire in an orderly sequence, occasional violations of the recruitment hierarchy have been observed in many species, particularly during rapid, oscillating movements (Azevedo et al., 2020; Desmedt and Godaux, 1981; Menelaou et al., 2022; Smith et al., 1980). Our finding that MNs receive an equal number of excitatory and inhibitory synapses, as originally speculated by Henneman and colleagues (Henneman et al., 1965), suggests a mechanism for inversions of the recruitment hierarchy. MNs with large dendritic fields and high conductances have faster time constants to better follow rapidly oscillating excitatory and inhibitory input, whereas smaller neurons may be both more sensitive to inhibition and slower to depolarize (Rall, 1959). Thus, smaller MNs at the bottom of the hierarchy may be differentially impacted by common inhibitory input to a motor module.

Recent work in primates also showed that stimulating neighboring cortical sites recruits different MNs within a motor pool, suggesting that descending input may flexibly subvert size-principle recruitment to accomplish different motor tasks (Marshall et al., 2022). Here, we found that intersegmental and descending neurons are more likely to selectively synapse onto subsets of MNs within modules than local neurons, which tend to contact all MNs within a module (**Figure 3E-F, Extended Data Figure 2**). These long-range pathways may serve to control ballistic leg movements that require subversion of the MN recruitment order, such as during escape behaviors (Azevedo et al., 2022; Kennedy and Broadie, 2018; von Reyn et al., 2014). Thus, we propose that the leg premotor network balances two seemingly opposed demands, reducing the dimensionality of local control within motor modules while maintaining the capacity to flexibly recruit MNs within a module to achieve specific motor tasks (Hug et al., 2023).

Past literature proposed a functional stratification of the wing steering MNs (Lindsay et al., 2017), in which some muscles are specialized for a constant and precise tuning of the wingstroke, while others are typically quiescent except when recruited to execute rapid maneuvers. In support of this scheme, we observed that descending neurons more often synapse onto MNs that are active during turning (**Extended Data Figure 1**). Unlike in the leg premotor network, local wing preMNs lack proportional connectivity, even to MNs within the same modules. We propose that this diverse range of common input patterns to wing MNs may have evolved to facilitate rapid and flexible control of the wing hinge. As connectomics is expanded to more and larger animals, it will be fascinating to compare how premotor networks have specialized to control diverse forms of locomotion (Barsotti et al., 2021).

Acknowledgements

This work was supported by a Searle Scholar Award, a Klingenstein-Simons Fellowship, a Pew Biomedical Scholar Award, a McKnight Scholar Award, a Sloan Research Fellowship, the New York Stem Cell Foundation, and a UW Innovation Award to JCT; a Genise Goldenson Award to WAL; NIH U19NS104655 to JCT and MD; NIH R01MH117808 to JCT, WAL, and HSS. JCT is a New York Stem Cell Foundation – Robertson Investigator. We thank Jim Truman, David Shepherd, Haluk Lacin, and Elizabeth Marin for assistance with hemilineage identification. We thank Greg Jefferis and Gwyneth Card for helpful discussions, and for their lab's contributions to proofreading in the FANC dataset. We thank members of the Tuthill and Dickinson Labs, Sama Ahmed, Bing Brunton, and Jim Truman for comments on the manuscript.

Methods

Reconstruction of premotor neurons (preMN) anatomy and connectivity

The automated segmentation of the Female Adult Nerve Cord electron microscopy dataset (FANC; (Phelps et al., 2021)), as well as the identification and reconstruction of leg and wing motor neurons (MNs), was described in a companion paper (Azevedo et al., 2022). To manually correct the automated segmentation of premotor neurons (preMNs), we used Google's collaborative Neuroglancer interface (Maitin-Shepard et al., 2021). We identified all objects in the automated segmentation that were predicted to synapse onto MNs. As a metric of both the quality of the segmentation and the speed of manual proofreading, initially 20% of the pre-synapses were associated with objects that had a soma. We proofread segments until >90% of all input to MNs was associated with either a cell body, or an identified descending or sensory process. The remaining inputs were categorized as fragment segments (**Extended Data Figure 1**). We deemed a neuron as "proofread" once its cell body was attached, its full backbone reconstructed, and as many branches as could be confidently attached.

Motor neuron volume and surface area were calculated using the statistics of the level 2 cache, which is the graph of "level 2 chunks" in the hierarchy of the PyChunkedGraph data structure (Dorkenwald et al., 2022; Schneider-Mizell et al., 2023). The computed level 2 cache maintains a representative central point in space, the volume, and the surface area for each level 2 chunk and these statistics are updated when new chunks are created due to proofreading edits.

Definition of cell classes

We classified all premotor neurons (preMNs) into five groups. Descending neurons had a process in the neck connective and no cell body in the VNC. Ascending neurons had a process in the neck connective and a cell body in the VNC. Sensory neurons had processes entering the VNC from peripheral nerves and no cell body in the VNC. The rest of the neurons were fully contained within the VNC. Leg preMNs were classified as local if all of their input synapses were within a bounding box containing the left T1 neuromere, and as intersegmental if they had input synapses outside the bounding box. Wing preMNs were classified as intersegmental if they had input synapses in any of the six leg neuropils or the abdominal neuropil (e.g. wing preMNs were considered local if they received input from the contralateral wing neuromere, haltere neuromeres, or neck neuromere). We did not split the wing neuropil into right and left sides because some wing MNs cross the midline. All preMNs were manually checked to make sure they were in the correct categories.

Definition of leg motor modules

We defined leg motor modules by combining knowledge of muscle targets with the cosine similarity metric. Cosine similarity was calculated using the cosine similarity method from the scikit-learn python package (**Figure 3**).

For simplicity, we label each module according to the phase of the step cycle–swing (orange) or stance (blue)–during which the module is most likely active (**Figure 1C, Figure 2C, Figure 3B**). The trochanter-femur joint is thought to be fused in flies, so we color the femur reductor module red to indicate its unknown function. Yellow indicates the module that controls the long tendon, or *retractor unguis*, that inserts on the claw at the tip of the tarsus to grip the substrate.

Our labeling scheme only considers module function during walking and should not be considered universal across behavioral contexts. When the fly is standing upright, for example, supporting the weight of the body requires contracting the trochanter extensor to supplement passive forces, assuming that passive forces in the leg are not sufficient (Hooper et al., 2009). During the stance phase of walking, flexion of the coxa-trochanter joint pulls the fly forward. Thus, during the stance phase, it is possible that both extensor and flexor muscle are contracting to balance the dual requirements of maintaining posture and moving forward. As a further example, the coxa swing module is composed of muscles that originate in the thorax and likely pull the coxa forward in slightly different directions, e.g. adduction vs. abduction. Consistent with this, the cosine similarity of all seven MNs (**Figure 3B**) appears to group into smaller clusters of anatomically related MNs with higher similarity. For simplicity, we include all seven MNs as one module,

but there are probably important differences related to adducting vs abducting the leg during the swing phase that allow the fly to turn during walking. Further work will be required to test the role of particular modules in posture and movement.

Definition of wing motor modules

MN similarity was calculated and clustered using the cosine similarity and agglomerative clustering methods from the scikit-learn python package.

The MNs that innervate power muscles were straightforward to define: the five MNs to dorsal longitudinal muscles (DLMs) clustered together and the seven MNs to dorsal ventral muscles (DVMs) clustered together. The "tension" cluster contains five of the six MNs to tension muscles, as the tpn MN, which innervates both tergopleural muscle fibers, had higher similarity with the steering MN iii1 than the other tension MNs.

Steering module A (tpn, iii1, iii3; cosine similarity = 0.34) was characterized as wing extension/increasing wingbeat amplitude based on correlations between iii1 muscle activity and wing kinematics (Melis and Dickinson, personal communication).

Steering module B (i1, i2, b3; cosine similarity mean = 0.4) was characterized as decreasing wingbeat amplitude because i1 fires during ipsilateral turns (Heide, 1975). Flies turn by decreasing the amplitude of the wingstroke on the inside of the turn (ipsilateral) while increasing the amplitude of the wingstroke on the outside of the turn.

Steering module C (b1, b2; cosine similarity = 0.7) was characterized as pitch control and wingstroke amplitude maintenance based on optogenetic manipulations in freely flying flies (Whitehead et al., 2022).

Steering module D (iv1, iv3, iv4, iii4; cosine similarity = 0.62) was not assigned a functional role.

Preference score

To compute the preference score for a preMN (**Figure 3E**), we summed the number of synapses onto each MN within a module and divided by the total synapses onto all MNs. For example, a preMN that makes 100 synapses onto wing MNs, 80 of which are onto different DLM MNs, would have a preference strength of 0.8.

In the wing, the DVM power module had the lowest percentage of input from module-preferring local preMNs (**Extended Data Figure 2**). This result is also reflected in the similarity matrices showing common input to DLMs and DVMs. DLMs have more input synapses than DVMs (**Extended Data Figure 1**), so common input to DLMs and DVMs tends to favor the DLM module overall.

Bootstrap analysis of proportional module connectivity

To test the importance of proportional connectivity in causing high MN similarity, we performed bootstrap shuffling of the connectivity, and compared the resulting MN similarity (**Extended Data Figure 4**). Specifically, for a set of MNs, j, in a particular module, and the preMNs, i, that prefer that module, we randomly permuted the synapse counts n_{ij} with respect to j, the MN identity. We then computed the pairwise MN cosine similarity and calculated the mean. The synapse counts were shuffled N=10,000 times and the distribution of the mean pairwise similarity was compared to the mean pairwise similarity for the real, unshuffled synapse counts. This test specifically asks, how often do we observe such high MN similarity, if the synapse counts are shuffled to break the tendency of preMN, *i*, to make proportionally more synapses onto the largest MNs?

We limited our analysis to comparing the largest neurons with the highest similarity. For example, we examined only the five main tibia flexors in the Tibia flex A pool, and excluded the accessory tibia flexors. If we instead included all MNs and shuffled the synapse counts across the entire module, accessory tibia flexor MNs would receive input from preMNs that do not ordinarily connect to those MNs, and tibia flexor MNs that ordinarily receive input from that preMN, now would not. This decreases the mean cosine similarity more than including only on the five main tibia flexors (not shown). Instead, we test the narrow proposition that, for MNs which all receive substantial and precise input from a set a preMNs, when that input is shuffled, the MNs become less similar.

PCA analysis of module connectivity

We define module connectivity as the matrix of synapse counts onto all of the MNs in a module, from the preMNs that preferentially target that module. We performed PCA on the module connectivity for each module using the scikit-learn PCA routines in python. The number of PCs for each module is the same as the number of MNs in the module. The first PC is the output weights onto MNs in the module that captures the most variance. By definition, the remaining PCs must be orthonormal and together capture the remaining variability in the module connectivity.

Identification of premotor hemilineages

Groups of VNC preMNs were first identified by the entry of their primary neurite into the neuropil. Primary neurite groups that bundled together were then identified as known hemilineages based on light microscopy images of sparse GAL4 lines, cell body position along the dorsal-ventral axis (Lacin et al., 2019; Meissner et al., 2020), and personal communication (Jim Truman, David Shepherd, Haluk Lacin, Elizabeth Marin). Not all of the clues are available for all of the neurite bundles. Of the 1184 local and intersegmental preMNs for the left wing MNs, 1103 were matched to a hemilineage (**Extended Data Figure 5**), which accounted for 94% of the VNC input to wing MNs. See **Supplemental Table 3** for links to view entire premotor populations of each hemilineage in Neuroglancer, an online tool for viewing connectomics datasets.

Of the 563 local leg preMNs, 533 were confidently assigned to a hemilineage, and 87 of the 279 intersegmental leg preMNs were assigned to a hemilineage, which accounted for 85% of the VNC input to the leg MNs.

The remaining 30 local preMNs have primary neurites that accompany MN bundles. Sixteen are bundled with the trochanter extensor neuron that has a dorsal soma (**Extended Data Figure 4B**), fourteen have anterior somas and are bundled with other MNs. Baek and Mann reported a clonal lineage, Lin E, that derived from a MN lineage and produced approximately 20 local neurons (Baek and Mann, 2009). We thus hypothesize that the untyped preMNs with anterior somas are likely Lin E and glutamatergic. We assigned glutamate to the preMNs with dorsal somas as well, since they also bundle with an MN. Our assignments will have to be confirmed experimentally, but we attempted to test the validity of our assignment through an analysis of the connectivity of local preMNs onto one another. We observed that cholinergic local preMNs did not contact other cholinergic preMNs that preferred the antagonist pool. If we assigned acetylcholine instead of glutamate to the untyped preMNs, we began to observe connections from cholinergic preMNs onto antagonist cholinergic preMNs. Feedforward antagonist inhibition is more physiologically plausible than feedforward antagonist excitation, giving us confidence that these untyped preMNs are likely glutamatergic.

Analysis of synergistic preMN connectivity

To analyze the tendency of preMNs from cholinergic hemilineages to contact non-preferred modules (**Figure 5F**), we calculated the number of synapses onto each module, divided by the sum of all synapses onto MNs. The module with the highest preference was the preferred module, as above, and the module with the second highest fraction we called the synergist module. Many of the preMNs contacted a single module (module preference=100%). For preMNs that contacted more than one module, 92% made most of those across-module connections onto either the tibia extend and flex modules, or the trochanter extend and flex modules. Thus, for simplicity when comparing the fraction of synapses onto synergist modules, we only compared connections onto the trochanter and tibia modules. For example, if the femur reductor module received the highest fraction of synapses after the preferred module, we ignored those connections and moved on to the highest fraction for either the trochanter or tibia modules.

Software and data availability

Data presented in the paper was analyzed from the CAVE materialization v604, timestamp 1684915801.222989. Annotated connectivity matrices (**Figure 2**) will be available as python Pandas data frames (https://pandas.pydata.org/) at the git-hub repository for this paper, https://github.com/tuthill-lab/Lesser_Azevedo_2023. Also available at the repository are scripts to recreate the analyses and figures in the paper, as well as scripts to recreate the connectivity matrices, for users authorized to interact with the CAVEclient. Links to public preMN and MN segmentations are available throughout the text, as well as in a document at the git-hub repository. All analysis was performed in Python 3.9 using custom code, making extensive use of CAVEclient (https://github.com/seung-lab/CAVEclient) and CloudVolume to interact with data infrastructure, and libraries Matplotlib, Numpy, Pandas, Scikit-learn, Scipy, stats-models and VTK for general computation, machine learning and data visualization. Additional code is available at https://github.com/htem/FANC_auto_recon, providing additional tutorials, code and documentation for interacting with FANC.

References Cited

Allen, A.M., Neville, M.C., Birtles, S., Croset, V., Treiber, C.D., Waddell, S., Goodwin, S.F., Mann, R.S., 2020. A single-cell transcriptomic atlas of the adult Drosophila ventral nerve cord. eLife 9, 1–32. https://doi.org/10.7554/eLife.54074

Atwood, H.L., Wiersma, C.A.G., 1967. Command Interneurons in the Crayfish Central Nervous System. J. Exp. Biol. 46, 249–261.

Azevedo, A., Lesser, E., Mark, B., Phelps, J., Elabbady, L., Kuroda, S., Sustar, A., Moussa, A., Kandelwal, A., Dallmann, C.J., Agrawal, S., Lee, S.-Y.J., Pratt, B., Cook, A., Skutt-Kakaria, K., Gerhard, S., Lu, R., Kemnitz, N., Lee, K., Halageri, A., Castro, M., Ih, D., Gager, J., Tammam, M., Dorkenwald, S., Collman, F., Schneider-Mizell, C., Brittain, D., Jordan, C.S., Dickinson, M., Pacureanu, A., Seung, H.S., Macrina, T., Lee, W.-C.A., Tuthill, J.C., 2022. Tools for comprehensive reconstruction and analysis of Drosophila motor circuits. https://doi.org/10.1101/2022.12.15.520299

Azevedo, A.W., Dickinson, E.S., Gurung, P., Venkatasubramanian, L., Mann, R.S., Tuthill, J.C., 2020. A size principle for recruitment of Drosophila leg motor neurons. eLife 9, e56754. https://doi.org/10.7554/eLife.56754

Baek, M., Mann, R.S., 2009. Lineage and Birth Date Specify Motor Neuron Targeting and Dendritic Architecture in Adult Drosophila. J. Neurosci. 29, 6904–6916. https://doi.org/10.1523/JNEUROSCI.1585-09.2009

Balaskas, N., Abbott, L.F., Jessell, T.M., Ng, D., 2019. Positional Strategies for Connection Specificity and Synaptic Organization in Spinal Sensory-Motor Circuits. Neuron 102, 1143-1156.e4. https://doi.org/10.1016/j.neuron.2019.04.008

Balint, C.N., Dickinson, M.H., 2001. The correlation between wing kinematics and steering muscle activity in the blowfly Calliphora vicina. J. Exp. Biol. 204, 4213–4226. https://doi.org/10.1242/jeb.204.24.4213

Barsotti, E., Correia, A., Cardona, A., 2021. Neural architectures in the light of comparative connectomics. Curr. Opin. Neurobiol. 71, 139–149. https://doi.org/10.1016/j.conb.2021.10.006

Bernshteĭn, N.A., 1967. The co-ordination and regulation of movements, [1st English ed.]. ed. Pergamon Press, Oxford.

Bidaye, S.S., Machacek, C., Wu, Y., Dickson, B.J., 2014. Neuronal Control of Drosophila Walking Direction. Science 344, 97–101. https://doi.org/10.1126/science.1249964

Binder, M.D., Bawa, P., Ruenzel, P., Henneman, E., 1983. Does orderly recruitment of motoneurons depend on the existence of different types of motor units? Neurosci. Lett. 36, 55–58. https://doi.org/10.1016/0304-3940(83)90485-8

Binder, M.D., Powers, R.K., Heckman, C.J., 2020. Nonlinear Input-Output Functions of Motoneurons. Physiol. Bethesda Md 35, 31–39. https://doi.org/10.1152/physiol.00026.2019

Boettiger, E.G., Furshpan, E., 1952. The mechanics of flight movements in diptera. Biol. Bull. 102, 200–211. https://doi.org/10.2307/1538368

Brierley, D. j., Rathore, K., VijayRaghavan, K., Williams, D. w., 2012. Developmental origins and architecture of Drosophila leg motoneurons. J. Comp. Neurol. 520, 1629–1649. https://doi.org/10.1002/cne.23003

Burke, R. e., Glenn, L. l., 1996. Horseradish peroxidase study of the spatial and electrotonic distribution of group Ia synapses on type-identified ankle extensor motoneurons in the cat. J. Comp. Neurol. 372, 465–485. https://doi.org/10.1002/(SICI)1096-9861(19960826)372:3<465::AID-CNE9>3.0.CO;2-0

Burrows, M., 1996. The Neurobiology of an Insect Brain. Oxford University Press, Oxford, New York.

Cook, S.J., Jarrell, T.A., Brittin, C.A., Wang, Y., Bloniarz, A.E., Yakovlev, M.A., Nguyen, K.C.Q., Tang, L.T.-H., Bayer, E.A., Duerr, J.S., Bülow, H.E., Hobert, O., Hall, D.H., Emmons, S.W., 2019. Whole-animal connectomes of both Caenorhabditis elegans sexes. Nature 571, 63–71. https://doi.org/10.1038/s41586-019-1352-7

Court, R., Namiki, S., Armstrong, J.D., Börner, J., Card, G., Costa, M., Dickinson, M., Duch, C., Korff, W., Mann, R., Merritt, D., Murphey, R.K., Seeds, A.M., Shirangi, T., Simpson, J.H., Truman, J.W., Tuthill, J.C., Williams, D.W., Shepherd, D., 2020. A Systematic Nomenclature for the Drosophila Ventral Nerve Cord. Neuron 107, 1071-1079.e2. https://doi.org/10.1016/j.neuron.2020.08.005

Cullheim, S., 1978. Relations between cell body size, axon diameter and axon conduction velocity of cat sciatic α-motoneurons stained with horseradish peroxidase. Neurosci. Lett. 8, 17–20. https://doi.org/10.1016/0304-3940(78)90090-3

Cullheim, S., Fleshman, J.W., Glenn, L.L., Burke, R.E., 1987. Membrane area and dendritic structure in type-identified triceps surae alpha motoneurons. J. Comp. Neurol. 255, 68–81. https://doi.org/10.1002/cne.902550106

De Luca, C.J., Erim, Z., 1994. Common drive of motor units in regulation of muscle force. Trends Neurosci. 17, 299–305. https://doi.org/10.1016/0166-2236(94)90064-7

Deora, T., Gundiah, N., Sane, S.P., 2017. Mechanics of the thorax in flies. J. Exp. Biol. 220, 1382–1395. https://doi.org/10.1242/jeb.128363

Desmedt, J.E., Godaux, E., 1981. Spinal Motoneuron Recruitment in Man: Rank Deordering with Direction but not with Speed of Voluntary Movement. Science 214, 933–936.

Dickinson, M.H., Lehmann, F.O., Götz, K.G., 1993. The active control of wing rotation by Drosophila. J. Exp. Biol. 182, 173–189. https://doi.org/10.1242/jeb.182.1.173

Dickinson, M.H., Tu, M.S., 1997. The Function of Dipteran Flight Muscle. Comp. Biochem. Physiol. A Physiol. 116, 223–238. https://doi.org/10.1016/S0300-9629(96)00162-4

Dorkenwald, S., McKellar, C.E., Macrina, T., Kemnitz, N., Lee, K., Lu, R., Wu, J., Popovych, S., Mitchell, E., Nehoran, B., Jia, Z., Bae, J.A., Mu, S., Ih, D., Castro, M., Ogedengbe, O., Halageri, A., Kuehner, K., Sterling, A.R., Ashwood, Z., Zung, J., Brittain, D., Collman, F., Schneider-Mizell, C., Jordan, C., Silversmith, W., Baker, C., Deutsch, D., Encarnacion-Rivera, L., Kumar, S., Burke, A., Bland, D., Gager, J., Hebditch, J., Koolman, S., Moore, M., Morejohn, S., Silverman, B., Willie, K., Willie, R., Yu, S.-C., Murthy, M., Seung, H.S., 2022. FlyWire: online community for whole-brain connectomics. Nat. Methods 19, 119–128. https://doi.org/10.1038/s41592-021-01330-0

Dudley, R., 2002. The Biomechanics of Insect Flight: Form, Function, Evolution. Princeton University Press.

Enriquez, J., Venkatasubramanian, L., Baek, M., Peterson, M., Aghayeva, U., Mann, R.S., 2015. Specification of individual adult motor neuron morphologies by combinatorial transcription factor codes. Neuron 86, 955–970. https://doi.org/10.1016/j.neuron.2015.04.011

Feng, K., Sen, R., Minegishi, R., Dübbert, M., Bockemühl, T., Büschges, A., Dickson, B.J., 2020. Distributed control of motor circuits for backward walking in Drosophila. Nat. Commun. 11, 6166. https://doi.org/10.1038/s41467-020-19936-x

Fry, S.N., Sayaman, R., Dickinson, M.H., 2003. The Aerodynamics of Free-Flight Maneuvers in Drosophila. Science 300, 495–498. https://doi.org/10.1126/science.1081944

Gabriel, J.P., Scharstein, H., Schmidt, J., Büschges, A., 2003. Control of flexor motoneuron activity during single leg walking of the stick insect on an electronically controlled treadwheel. J. Neurobiol. 56, 237–251. https://doi.org/10.1002/neu.10237

Graham, K.M., Scott, S.H., 2003. Morphometry of macaca mulatta forelimb. III. moment arm of shoulder and elbow muscles. J. Morphol. 255, 301–314. https://doi.org/10.1002/jmor.10064

Guan, W., Bellemin, S., Bouchet, M., Venkatasubramanian, L., Guillermin, C., Laurençon, A., Kabir, C., Darnas, A., Godin, C., Urdy, S., Mann, R.S., Enriquez, J., 2022. Post-transcriptional regulation of transcription factor codes in immature neurons drives neuronal diversity. Cell Rep. 39. https://doi.org/10.1016/j.celrep.2022.110992

Harris, R.M., Pfeiffer, B.D., Rubin, G.M., Truman, J.W., 2015. Neuron hemilineages provide the functional ground plan for the Drosophila ventral nervous system. eLife 4, e04493. https://doi.org/10.7554/eLife.04493

Heide, G., 1983. Neural mechanisms of flight control in Diptera. BIONA-Rep. 2, 35–52.

Heide, G., 1975. Properties of a motor output system involved in the optomotor response in flies. Biol. Cybern. 20, 99–112. https://doi.org/10.1007/BF00327047

Heide, G., Götz, K.G., 1996. Optomotor control of course and altitude in Drosophila melanogaster is correlated with distinct activities of at least three pairs of flight steering muscles. J. Exp. Biol. 199, 1711–1726. https://doi.org/10.1242/jeb.199.8.1711

Henneman, E., 1957. Relation between Size of Neurons and Their Susceptibility to Discharge. Science 126, 1345–1347. https://doi.org/10.1126/science.126.3287.1345

Henneman, E., Somjen, G., Carpenter, D.O., 1965. Excitability and inhibitibility of motoneurons of different sizes. J. Neurophysiol. 28, 599–620. https://doi.org/10.1152/jn.1965.28.3.599

Hill, A.A.V., Cattaert, D., 2008. Recruitment in a heterogeneous population of motor neurons that innervates the depressor muscle of the crayfish walking leg muscle. J. Exp. Biol. 211, 613–629. https://doi.org/10.1242/jeb.006270

Hodson-Tole, E.F., Wakeling, J.M., 2009. Motor unit recruitment for dynamic tasks: current understanding and future directions. J. Comp. Physiol. B 179, 57–66. https://doi.org/10.1007/s00360-008-0289-1

Hooper, S.L., Guschlbauer, C., Blümel, M., Rosenbaum, P., Gruhn, M., Akay, T., Büschges, A., 2009. Neural Control of Unloaded Leg Posture and of Leg Swing in Stick Insect, Cockroach, and Mouse Differs from That in Larger Animals. J. Neurosci. 29, 4109–4119. https://doi.org/10.1523/JNEUROSCI.5510-08.2009

Hörnschemeyer, T., 2002. Phylogenetic significance of the wing-base of the Holometabola (Insecta). Zool. Scr. 31, 17–29. https://doi.org/10.1046/j.0300-3256.2001.00086.x

Hoyle, G., 1983. Muscles and their neural control. New York : Wiley.

Hoyle, G., 1955. The anatomy and innervation of locust skeletal muscle. Proc. R. Soc. Lond. Ser. B - Biol. Sci. 143, 281–292. https://doi.org/10.1098/rspb.1955.0011

Hug, F., Avrillon, S., Ibáñez, J., Farina, D., 2023. Common synaptic input, synergies and size principle: Control of spinal motor neurons for movement generation. J. Physiol. 601, 11–20. https://doi.org/10.1113/JP283698

Kennedy, T., Broadie, K., 2018. Newly Identified Electrically Coupled Neurons Support Development of the Drosophila Giant Fiber Model Circuit. eNeuro 5, ENEURO.0346-18.2018. https://doi.org/10.1523/ENEURO.0346-18.2018

Kernell, D., 2006. The Motoneurone and its Muscle Fibres. Oxford University Press.

Kernell, D., Zwaagstra, B., 1989. Size and remoteness: two relatively independent parameters of dendrites, as studied for spinal motoneurones of the cat. J. Physiol. 413, 233–254. https://doi.org/10.1113/jphysiol.1989.sp017651

Kiehn, O., 2016. Decoding the organization of spinal circuits that control locomotion. Nat. Rev. Neurosci. 17, 224–238. https://doi.org/10.1038/nrn.2016.9

Kukalova-Peck, J., 1978. Origin and evolution of insect wings and their relation to metamorphosis, as documented by the fossil record. J. Morphol. 156, 53–125. https://doi.org/10.1002/jmor.1051560104

Lacin, H., Chen, H.-M., Long, X., Singer, R.H., Lee, T., Truman, J.W., 2019. Neurotransmitter identity is acquired in a lineage-restricted manner in the Drosophila CNS. eLife 8. https://doi.org/10.7554/eLife.43701

Lehmann, F.-O., Bartussek, J., 2017. Neural control and precision of flight muscle activation in Drosophila. J. Comp. Physiol. A Neuroethol. Sens. Neural. Behav. Physiol. 203, 1. https://doi.org/10.1007/s00359-016-1133-9

Li, H., Janssens, J., Waegeneer, M.D., Kolluru, S.S., Davie, K., Gardeux, V., Saelens, W., David, F.P.A., Brbić, M., Spanier, K., Leskovec, J., McLaughlin, C.N., Xie, Q., Jones, R.C., Brueckner, K., Shim, J., Tattikota, S.G., Schnorrer, F., Rust, K., Nystul, T.G., Carvalho-Santos, Z., Ribeiro, C., Pal, S., Mahadevaraju, S., Przytycka, T.M., Allen, A.M., Goodwin, S.F., Berry, C.W., Fuller, M.T., White-Cooper, H., Matunis, E.L., DiNardo, S., Galenza, A., O'Brien, L.E., Dow, J.A.T., Consortium§, F.C.A., Jasper, H., Oliver, B., Perrimon, N., Deplancke, B., Quake, S.R., Luo, L., Aerts, S., Agarwal, D., Ahmed-Braimah, Y., Arbeitman, M., Ariss, M.M., Augsburger, J., Ayush, K., Baker, C.C., Banisch, T., Birker, K., Bodmer, R., Bolival, B., Brantley, S.E., Brill, J.A., Brown, N.C., Buehner, N.A., Cai, X.T., Cardoso-Figueiredo, R., Casares, F., Chang, A., Clandinin, T.R., Crasta, S., Desplan, C., Detweiler, A.M., Dhakan, D.B., Donà, E., Engert, S., Floc'hlay, S., George, N., González-Segarra, A.J., Groves, A.K., Gumbin, S., Guo, Y., Harris, D.E., Heifetz, Y., Holtz, S.L., Horns, F., Hudry, B., Hung, R.-J., Jan, Y.N., Jaszczak, J.S., Jefferis, G.S.X.E., Karkanias, J., Karr, T.L., Katheder, N.S., Kezos, J., Kim, A.A., Kim, S.K., Kockel, L., Konstantinides, N., Kornberg, T.B., Krause, H.M., Labott, A.T., Laturney, M., Lehmann, R., Leinwand, S., Li, J., Li, J.S.S., Li, Kai, Li, Ke, Li, L., Li, T., Litovchenko, M., Liu, H.-H., Liu, Y., Lu, T.-C., Manning, J., Mase, A., Matera-Vatnick, M., Matias, N.R., McDonough-Goldstein, C.E., McGeever, A., McLachlan, A.D., Moreno-Roman, P., Neff, N., Neville, M., Ngo, S., Nielsen, T., O'Brien, C.E., Osumi-Sutherland, D., Özel, M.N., Papatheodorou, I., Petkovic, M., Pilgrim, C., Pisco, A.O., Reisenman, C., Sanders, E.N., Santos, G. dos, Scott, K., Sherlekar, A., Shiu, P., Sims, D., Sit, R.V., Slaidina, M., Smith, H.E., Sterne, G., Su, Y.-H., Sutton, D., Tamayo, M., Tan, M., Tastekin, I., Treiber, C., Vacek, D., Vogler, G., Waddell, S., Wang, W., Wilson, R.I., Wolfner, M.F., Wong, Y.-C.E., Xie, A., Xu, J., Yamamoto, S., Yan, J., Yao, Z., Yoda, K., Zhu, R., Zinzen, R.P., 2022. Fly Cell Atlas: A single-nucleus transcriptomic atlas of the adult fruit fly. Science. https://doi.org/10.1126/science.abk2432

Lillicrap, T.P., Scott, S.H., 2013. Preference Distributions of Primary Motor Cortex Neurons Reflect Control Solutions Optimized for Limb Biomechanics. Neuron 77, 168–179. https://doi.org/10.1016/j.neuron.2012.10.041

Lindsay, T., Sustar, A., Dickinson, M., 2017. The Function and Organization of the Motor System Controlling Flight Maneuvers in Flies. Curr. Biol. CB 27, 345–358. https://doi.org/10.1016/j.cub.2016.12.018

Lobato-Rios, V., Ramalingasetty, S.T., Özdil, P.G., Arreguit, J., Ijspeert, A.J., Ramdya, P., 2022. NeuroMechFly, a neuromechanical model of adult Drosophila melanogaster. Nat. Methods 19, 620–627. https://doi.org/10.1038/s41592-022-01466-7

Maitin-Shepard, J., Baden, A., Silversmith, W., Perlman, E., Collman, F., Blakely, T., Funke, J., Jordan, C., Falk, B., Kemnitz, N., tingzhao, Roat, C., Castro, M., Jagannathan, S., moenigin, Clements, J., Hoag, A., Katz, B., Parsons, D., Wu, J., Kamentsky, L., Chervakov, P., Hubbard, P., Berg, S., Hoffer, J., Halageri, A., Machacek, C., Mader, K., Roeder, L., Li, P.H., 2021. google/neuroglancer: https://doi.org/10.5281/zenodo.5573294

Mark, B., Lai, S.-L., Zarin, A.A., Manning, L., Pollington, H.Q., Litwin-Kumar, A., Cardona, A., Truman, J.W., Doe, C.Q., 2021. A developmental framework linking neurogenesis and circuit formation in the Drosophila CNS [WWW Document]. eLife. https://doi.org/10.7554/eLife.67510

Marshall, N.J., Glaser, J.I., Trautmann, E.M., Amematsro, E.A., Perkins, S.M., Shadlen, M.N., Abbott, L.F., Cunningham, J.P., Churchland, M.M., 2022. Flexible neural control of motor units. Nat. Neurosci. 25, 1492–1504. https://doi.org/10.1038/s41593-022-01165-8

McLean, D.L., Dougherty, K.J., 2015. Peeling back the layers of locomotor control in the spinal cord. Curr. Opin. Neurobiol. 33, 63–70. https://doi.org/10.1016/j.conb.2015.03.001

McLean, D.L., Fetcho, J.R., 2009. Spinal Interneurons Differentiate Sequentially from Those Driving the Fastest Swimming Movements in Larval Zebrafish to Those Driving the Slowest Ones. J. Neurosci. 29, 13566–13577. https://doi.org/10.1523/JNEUROSCI.3277-09.2009

Mcphedran, A.M., Wuerker, R.B., Henneman, E., 1965. Properties of motor units in a homogeneous red muscle (soleus) of the cat. J. Neurophysiol. 28, 71–84. https://doi.org/10.1152/jn.1965.28.1.71

Meissner, G.W., Dorman, Z., Nern, A., Forster, K., Gibney, T., Jeter, J., Johnson, L., He, Y., Lee, K., Melton, B., Yarbrough, B., Clements, J., Goina, C., Otsuna, H., Rokicki, K., Svirskas, R.R., Aso, Y., Card, G.M., Dickson, B.J., Ehrhardt, E., Goldammer, J., Ito, M., Korff, W., Minegishi, R., Namiki, S., Rubin, G.M., Sterne, G., Wolff, T., Malkesman, O., Team, F.P., 2020. An image resource of subdivided Drosophila GAL4-driver expression patterns for neuron-level searches. https://doi.org/10.1101/2020.05.29.080473

Mendell, L.M., Henneman, E., 1971. Terminals of single Ia fibers: location, density, and distribution within a pool of 300 homonymous motoneurons. J. Neurophysiol. 34, 171–187. https://doi.org/10.1152/jn.1971.34.1.171

Menelaou, E., Kishore, S., McLean, D.L., 2022. Mixed synapses reconcile violations of the size principle in zebrafish spinal cord. eLife 11, e64063. https://doi.org/10.7554/eLife.64063

Milner-Brown, H.S., Stein, R.B., Yemm, R., 1973. The orderly recruitment of human motor units during voluntary isometric contractions. J. Physiol. 230, 359–370. https://doi.org/10.1113/jphysiol.1973.sp010192

Miyan, J.A., Ewing, A.W., 1985. How Diptera move their wings: a re-examination of the wing base articulation and muscle systems concerned with flight. Philos. Trans. R. Soc. Lond. B Biol. Sci. 311, 271–302. https://doi.org/10.1098/rstb.1985.0154

Monster, A.W., Chan, H., 1977. Isometric force production by motor units of extensor digitorum communis muscle in man. J. Neurophysiol. 40, 1432–1443. https://doi.org/10.1152/jn.1977.40.6.1432

Muijres, F.T., Elzinga, M.J., Melis, J.M., Dickinson, M.H., 2014. Flies Evade Looming Targets by Executing Rapid Visually Directed Banked Turns. Science 344, 172–177. https://doi.org/10.1126/science.1248955

Nachtigall, W., Wilson, D.M., 1967. Neuro-Muscular Control of Dipteran Flight. J. Exp. Biol. 47, 77–97. https://doi.org/10.1242/jeb.47.1.77

Namiki, S., Dickinson, M.H., Wong, A.M., Korff, W., Card, G.M., 2018. The functional organization of descending sensory-motor pathways in Drosophila. eLife 7, e34272. https://doi.org/10.7554/eLife.34272

Newland, P.L., Kondoh, Y., 1997. Dynamics of Neurons Controlling Movements of a Locust Hind Leg II. Flexor Tibiae Motor Neurons. J. Neurophysiol. 77, 1731–1746. https://doi.org/10.1152/jn.1997.77.4.1731

Ohyama, T., Schneider-Mizell, C.M., Fetter, R.D., Aleman, J.V., Franconville, R., Rivera-Alba, M., Mensh, B.D., Branson, K.M., Simpson, J.H., Truman, J.W., Cardona, A., Zlatic, M., 2015. A multilevel multimodal circuit enhances action selection in Drosophila. Nature 520, 633–639. https://doi.org/10.1038/nature14297

Örnung, G., Ottersen, O.P., Cullheim, S., Ulfhake, B., 1998. Distribution of glutamate-, glycine- and GABA-immunoreactive nerve terminals on dendrites in the cat spinal motor nucleus. Exp. Brain Res. 118, 517–532. https://doi.org/10.1007/s002210050308

O'Sullivan, A., Lindsay, T., Prudnikova, A., Erdi, B., Dickinson, M., von Philipsborn, A.C., 2018. Multifunctional Wing Motor Control of Song and Flight. Curr. Biol. CB 28, 2705-2717.e4. https://doi.org/10.1016/j.cub.2018.06.038

Phelps, J.S., Hildebrand, D.G.C., Graham, B.J., Kuan, A.T., Thomas, L.A., Nguyen, T.M., Buhmann, J., Azevedo, A.W., Sustar, A., Agrawal, S., Liu, M., Shanny, B.L., Funke, J., Tuthill, J.C., Lee, W.-C.A., 2021. Reconstruction of motor control circuits in adult Drosophila using automated transmission electron microscopy. Cell 184, 759-774.e18. https://doi.org/10.1016/j.cell.2020.12.013

Pringle, J.W.S., 1957. Insect Flight. Cambridge University Press.

Pringle, J.W.S., 1949. The excitation and contraction of the flight muscles of insects. J. Physiol. 108, 226–232. https://doi.org/10.1113/jphysiol.1949.sp004326

Radnikow, G., Bässler, U., 1991. Function of a Muscle Whose Apodeme Travels Through a Joint Moved by Other Muscles: Why the Retractor Unguis Muscle in Stick Insects is Tripartite and has no Antagonist. J. Exp. Biol. 157, 87–99. https://doi.org/10.1242/jeb.157.1.87

Rall, W., 1959. Branching dendritic trees and motoneuron membrane resistivity. Exp. Neurol. 1, 491–527. https://doi.org/10.1016/0014-4886(59)90046-9

Ronzano, R., Skarlatou, S., Barriga, B.K., Bannatyne, B.A., Bhumbra, G.S., Foster, J.D., Moore, J.D., Lancelin, C., Pocratsky, A.M., Özyurt, M.G., Smith, C.C., Todd, A.J., Maxwell, D.J., Murray, A.J., Pfaff, S.L., Brownstone, R.M., Zampieri, N., Beato, M., 2022. Spinal premotor interneurons controlling antagonistic muscles are spatially intermingled. eLife 11, e81976. https://doi.org/10.7554/eLife.81976

Sasaki, K., Burrows, M., 1998. Innervation pattern of a pool of nine excitatory motor neurons in the flexor tibiae muscle of a locust hind leg. J. Exp. Biol. 201, 1885–1893.

Scheibel, M.E., Schiebel, A.B., 1969. Terminal patterns in cat spinal cord III. Primary afferent collaterals. Brain Res. 13, 417–443. https://doi.org/10.1016/0006-8993(69)90258-3

Schneider-Mizell, C.M., Bodor, A., Brittain, D., Buchanan, J., Bumbarger, D.J., Elabbady, L., Kapner, D., Kinn, S., Mahalingam, G., Seshamani, S., Suckow, S., Takeno, M., Torres, R., Yin, W., Dorkenwald, S., Bae, J.A., Castro, M.A., Fahey, P.G., Froudakis, E., Halageri, A., Jia, Z., Jordan, C., Kemnitz, N., Lee, K., Li, K., Lu, R., Macrina, T., Mitchell, E., Mondal, S.S., Mu, S., Nehoran, B., Papadopoulos, S., Patel, S., Pitkow, X., Popovych, S., Silversmith, W., Sinz, F.H., Turner, N.L., Wong, W., Wu, J., Yu, S., Consortium, Mic., Reimer, J., Tolias, A.S., Seung, H.S., Reid, R.C., Collman, F., Costa, N.M. da, 2023. Cell-type-specific inhibitory circuitry from a connectomic census of mouse visual cortex. https://doi.org/10.1101/2023.01.23.525290

Schnell, B., Ros, I., Dickinson, M.H., 2017. A descending neuron correlated with the rapid steering maneuvers of flying Drosophila. Curr. Biol. CB 27, 1200–1205. https://doi.org/10.1016/j.cub.2017.03.004

Shepherd, D., Sahota, V., Court, R., Williams, D.W., Truman, J.W., 2019. Developmental organization of central neurons in the adult Drosophila ventral nervous system. J. Comp. Neurol. https://doi.org/10.1002/cne.24690

Sherrington, C.S., 1906. The integrative action of the nervous system, Yale paperbound ; Y-35. Yale University Press, New Haven.

Shiozaki, H.M., Wang, K., Lillvis, J.L., Xu, M., Dickson, B.J., Stern, D.L., 2022. Neural coding of distinct motor patterns during Drosophila courtship song. https://doi.org/10.1101/2022.12.14.520499

Smith, J.L., Betts, B., Edgerton, V.R., Zernicke, R.F., 1980. Rapid ankle extension during paw shakes: selective recruitment of fast ankle extensors. J. Neurophysiol. 43, 612–620. https://doi.org/10.1152/jn.1980.43.3.612

Ting, L.H., Macpherson, J.M., 2005. A Limited Set of Muscle Synergies for Force Control During a Postural Task. J. Neurophysiol. 93, 609–613. https://doi.org/10.1152/jn.00681.2004

Todorov, E., Li, W., Pan, X., 2005. From task parameters to motor synergies: A hierarchical framework for approximately-optimal control of redundant manipulators. J. Robot. Syst. 22, 691–710. https://doi.org/10.1002/rob.20093

Truman, J.W., Schuppe, H., Shepherd, D., Williams, D.W., 2004. Developmental architecture of adult-specific lineages in the ventral CNS of Drosophila. Development 131, 5167–5184. https://doi.org/10.1242/dev.01371

Tu, M.S., Dickinson, M.H., 1996. The control of wing kinematics by two steering muscles of the blowfly (Calliphora vicina). J. Comp. Physiol. A 178, 813–830. https://doi.org/10.1007/BF00225830

Tu, M.S., Dickinson, M.H., 1994. Modulation of Negative Work Output from a Steering Muscle of the Blowfly Calliphora Vicina. J. Exp. Biol. 192, 207–224. https://doi.org/10.1242/jeb.192.1.207

Tuthill, J.C., Wilson, R.I., 2016. Mechanosensation and Adaptive Motor Control in Insects. Curr. Biol. CB 26, R1022–R1038. https://doi.org/10.1016/j.cub.2016.06.070

Ulfhake, B., Cullheim, S., 1988. Postnatal development of cat hind limb motoneurons. III: Changes in size of motoneurons supplying the triceps surae muscle. J. Comp. Neurol. 278, 103–120. https://doi.org/10.1002/cne.902780107

Venkatasubramanian, L., Guo, Z., Xu, S., Tan, L., Xiao, Q., Nagarkar-Jaiswal, S., Mann, R.S., 2019. Stereotyped terminal axon branching of leg motor neurons mediated by IgSF proteins DIP-α and Dpr10. eLife 8. https://doi.org/10.7554/eLife.42692

von Reyn, C.R., Breads, P., Peek, M.Y., Zheng, G.Z., Williamson, W.R., Yee, A.L., Leonardo, A., Card, G.M., 2014. A spike-timing mechanism for action selection. Nat. Neurosci. 17, 962–970. https://doi.org/10.1038/nn.3741

Wen, Q., Po, M.D., Hulme, E., Chen, S., Liu, X., Kwok, S.W., Gershow, M., Leifer, A.M., Butler, V., Fang-Yen, C., Kawano, T., Schafer, W.R., Whitesides, G., Wyart, M., Chklovskii, D.B., Zhen, M., Samuel, A.D.T., 2012. Proprioceptive Coupling within Motor Neurons Drives C. elegans Forward Locomotion. Neuron 76, 750–761. https://doi.org/10.1016/j.neuron.2012.08.039

Whitehead, S.C., Leone, S., Lindsay, T., Meiselman, M.R., Cowan, N.J., Dickinson, M.H., Yapici, N., Stern, D.L., Shirangi, T., Cohen, I., 2022. Neuromuscular embodiment of feedback control elements in Drosophila flight. Sci. Adv. 8, eabo7461. https://doi.org/10.1126/sciadv.abo7461

Williams, C.M., Williams, M.V., 1943. The flight muscles of Drosophila repleta. J. Morphol. 72, 589–599. https://doi.org/10.1002/jmor.1050720308

Winding, M., Pedigo, B.D., Barnes, C.L., Patsolic, H.G., Park, Y., Kazimiers, T., Fushiki, A., Andrade, I.V., Khandelwal, A., Valdes-Aleman, J., Li, F., Randel, N., Barsotti, E., Correia, A., Fetter, R.D., Hartenstein, V., Priebe, C.E., Vogelstein, J.T., Cardona, A., Zlatic, M., 2023. The connectome of an insect brain. Science 379, eadd9330. https://doi.org/10.1126/science.add9330

Winding, M., Pedigo, B.D., Barnes, C.L., Patsolic, H.G., Park, Y., Kazimiers, T., Fushiki, A., Andrade, I.V., Khandelwal, A., Valdes-Aleman, J., Li, F., Randel, N., Barsotti, E., Correia, A., Fetter, R.D., Hartenstein, V., Priebe, C.E., Vogelstein, J.T., Cardona, A., Zlatic, M., 2022. The connectome of an insect brain. https://doi.org/10.1101/2022.11.28.516756

Wuerker, R.B., McPhedran, A.M., Henneman, E., 1965. Properties of motor units in a heterogeneous pale muscle (m. gastrocnemius) of the cat. J. Neurophysiol. 28, 85–99. https://doi.org/10.1152/jn.1965.28.1.85

Zarin, A.A., Mark, B., Cardona, A., Litwin-Kumar, A., Doe, C.Q., 2019. A multilayer circuit architecture for the generation of distinct locomotor behaviors in Drosophila. eLife 8, e51781. https://doi.org/10.7554/eLife.51781

Zhang, N., Simpson, J.H., 2022. A pair of commissural command neurons induces Drosophila wing grooming. iScience 25, 103792. https://doi.org/10.1016/j.isci.2022.103792

Zheng, Z., Lauritzen, J.S., Perlman, E., Robinson, C.G., Nichols, M., Milkie, D., Torrens, O., Price, J., Fisher, C.B., Sharifi, N., Calle-Schuler, S.A., Kmecova, L., Ali, I.J., Karsh, B., Trautman, E.T., Bogovic, J.A., Hanslovsky, P., Jefferis, G.S.X.E., Kazhdan, M., Khairy, K., Saalfeld, S., Fetter, R.D., Bock, D.D., 2018. A Complete Electron Microscopy Volume of the Brain of Adult Drosophila melanogaster. Cell 174, 730-743.e22. https://doi.org/10.1016/j.cell.2018.06.019

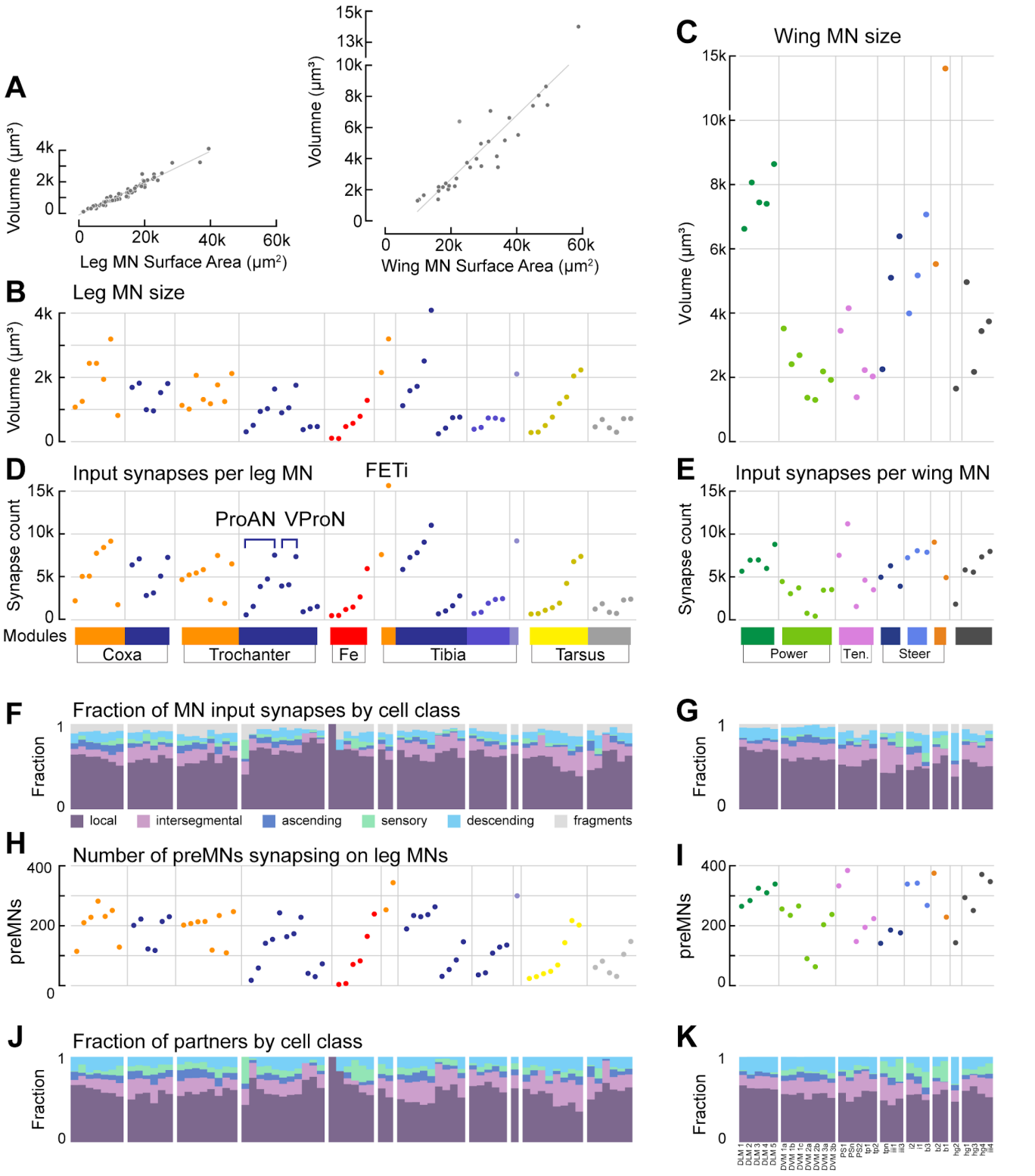

Extended Data Figure 1. Detailed properties of individual leg and wing MNs. (**A**) MN volume vs. surface area for leg MNs (left) and wing MNs (right). Wing MNs tend to have thicker neurites, explaining the steeper relationship. The thick b1 wing steering MN is the outlier. (**B**) Cell volume of each MN controlling the left front leg. MNs are grouped by motor modules (colors and vertical gray lines). See Supplemental Table 1 for links to view MNs grouped by modules. (**C**) Cell volume of each MN controlling the wing, including thoracic muscles that power the wingstroke. MNs are grouped by motor module. (**D**) Number of input synapses on each leg MN. MNs are ordered as in **C**. (**E**) Number of input synapses on each wing MN. MNs are ordered as in **C**. (**F**) Fraction of synapses on each leg MN broken down by cell class. (**G**) Fraction of synapses on each wing MN broken down by cell class. (**H**) Number of preMNs presynaptic to each leg MN. (**I**) Number of preMNs presynaptic to each wing MN. (**J**) Fraction of proofread presynaptic partners to each leg MN broken down by cell class. Fragments are not included. (**K**) Fraction of proofread presynaptic partners to each wing MN broken down by cell class.

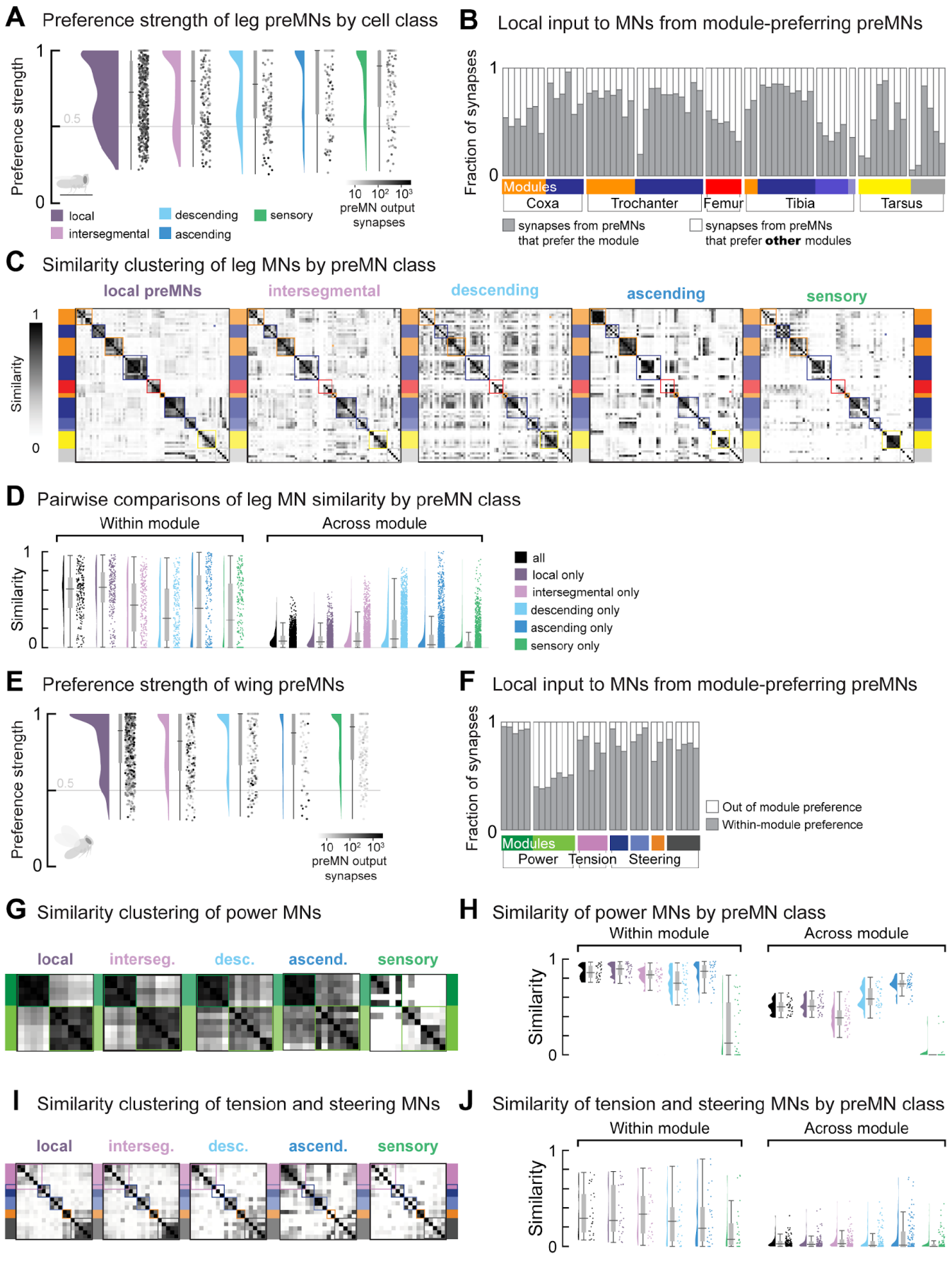
A
Preference strength of leg preMNs by cell class
Preference strength
1
0.5
0
local
intersegmental
descending
ascending
sensory
10 10² 10³
preMN output synapses
B
Local input to MNs from module-preferring preMNs
Fraction of synapses
1
0
Modules
Coxa
Trochanter
Femur
Tibia
Tarsus
synapses from preMNs that prefer the module
synapses from preMNs that prefer other modules
C
Similarity clustering of leg MNs by preMN class
local preMNs
intersegmental
descending
ascending
sensory
Similarity
1
0
D
Pairwise comparisons of leg MN similarity by preMN class
Within module
Across module
Similarity
1
0
all
local only
intersegmental only
descending only
ascending only
sensory only
E
Preference strength of wing preMNs
Preference strength
1
0.5
0
10 10² 10³
preMN output synapses
F
Local input to MNs from module-preferring preMNs
Fraction of synapses
1
0
Modules
Power
Tension
Steering
Out of module preference
Within-module preference
G
Similarity clustering of power MNs
local
interseg.
desc.
ascend.
sensory
H
Similarity of power MNs by preMN class
Within module
Across module
Similarity
1
0
I
Similarity clustering of tension and steering MNs
local
interseg.
desc.
ascend.
sensory
J
Similarity of tension and steering MNs by preMN class
Within module
Across module
Similarity
1
0

Extended Data Figure 2. Local premotor neurons target motor modules. (**A**) Module preference for individual preMNs targeting leg MNs, separated by cell class of preMNs. Module preference is defined as the (sum of the number of synapses onto each MNs in a module) / (total number of synapses onto all MNs). Dots represent individual local preMNs, with grayscale indicating the total number of synapses on a log scale. (**B**) Fraction of MN input synapses (each bar) from local preMNs that prefer that MN's module (gray), vs. or prefers a different module (white). This fraction is below 50% for the coxa swing module (left-most module), reflecting the subdivision of this module into submodules (**Methods**). Other MNs below 50% include the tibia flex B and C module MNs, and the two tarsus neurons that did not show synergistic MN similarity to tibia flexion modules. (**C**) Cosine similarity matrices for leg MNs, calculated on synapses from preMNs of each cell class. Axes are symmetrical, modules are ordered from proximal to distal along the leg, as in **Figure 3**. We observed higher cross-module similarity, ~0.3-0.5, when considering only descending preMNs. MNs in different modules rarely receive input from the same DNs, but when they do, e.g. the DN shown in **Figure 2B**, those few connections lead to a relatively high cosine similarity. (**D**) Pairwise similarity of MNs within modules, when considering all preMNs (black), or just a single class, as illustrated by the similarity matrices in **C**. (**E**) Module preference for individual preMNs targeting wing MNs, as shown in **A** for leg MNs. (**F**) Fraction of input synapses on wing MNs from local preMNs that preferentially target each MN's module (gray) vs a different module (white). (**G**) Similarity matrices for indirect (power) wing MNs constrained to preMNs of each cell class. Indirect muscles are divided into two antagonistic modules: dorsal longitudinal muscles (DLMs, dark green) and dorso-ventral muscles (DVMs, light green). They share common input from all cell classes except sensory axons, from which they receive few synapses. (**H**) Pairwise similarity of indirect MNs within modules, constrained to premotor input from distinct cell classes. (**I**) Similarity matrices for tension and direct (steering) MNs. (**J**) Pairwise similarity of indirect MNs within modules, constrained to premotor input from distinct cell classes. Colors are indicated in **D**.

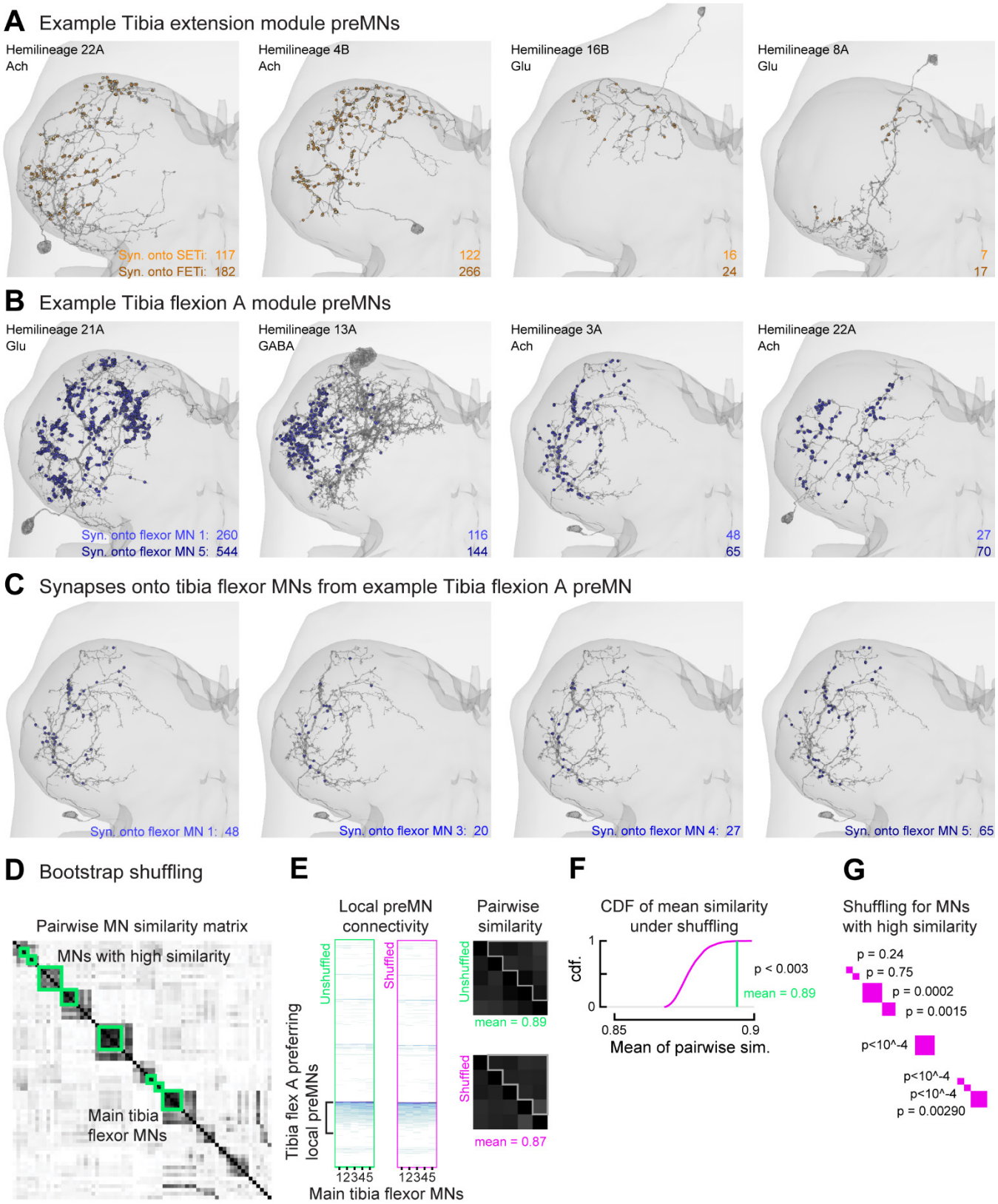
A Example Tibia extension module preMNs
Hemilineage 22A
Ach
Syn. onto SETi: 117
Syn. onto FETi: 182
Hemilineage 4B
Ach
122
266
Hemilineage 16B
Glu
16
24
Hemilineage 8A
Glu
7
17
B Example Tibia flexion A module preMNs
Hemilineage 21A
Glu
Syn. onto flexor MN 1: 260
Syn. onto flexor MN 5: 544
Hemilineage 13A
GABA
116
144
Hemilineage 3A
Ach
48
65
Hemilineage 22A
Ach
27
70
C Synapses onto tibia flexor MNs from example Tibia flexion A preMN
Syn. onto flexor MN 1: 48
Syn. onto flexor MN 3: 20
Syn. onto flexor MN 4: 27
Syn. onto flexor MN 5: 65
D Bootstrap shuffling
Pairwise MN similarity matrix
MNs with high similarity
Main tibia flexor MNs
E
Local preMN connectivity
Pairwise similarity
Unshuffled
Shuffled
Tibia flex A preferring local preMNs
12345
12345
Main tibia flexor MNs
mean = 0.89
mean = 0.87
F
CDF of mean similarity under shuffling
cdf.
1
0
p < 0.003
mean = 0.89
0.85
0.9
Mean of pairwise sim.
G
Shuffling for MNs with high similarity
p = 0.24
p = 0.75
p = 0.0002
p = 0.0015
p<10^-4
p<10^-4
p<10^-4
p = 0.00290

Extended Data Figure 3. Proportional connectivity: example preMNs, their synapses onto motor modules, and the importance of proportional connectivity to MN similarity. (**A**) The location of synapses (spheres) from example preMNs that preferentially synapse onto the SETi (light orange) and FETi (dark orange) MNs in the Tibia Extend module. Each preMN has a different morphology and makes more synapses onto FETi than onto SETi. (**B**) Example preMNs that preferentially synapse onto the five tibia flexor MNs in the Tibia Flex A module (different shades of blue spheres). (**C**) A single example preMN from **B**, showing the locations of synapses onto four of the five tibia flexor MNs in the module. The preMN makes more synapses onto the largest neurons, with extra synapses distributed throughout the processes. See **Supplemental Table 2** for links to view entire premotor populations that prefer particular modules in Neuroglancer, an online tool for viewing connectomics datasets. (**D**) Bootstrap shuffling of module connectivity (see **Methods** for details). We consider only the largest neurons with the highest similarity (green squares), where high MN similarity reflects preMNs that synapse onto each MN in the module, as in **A-C**. (**E**) Left, the unshuffled synapse counts from all local preMNs onto the Tibia Flex A MNs; middle, the same matrix with example shuffled synapse counts from the module-targeting preMNs; right, the resulting MN similarity matrices, highlighting the pairwise similarities in the upper triangle. (**F**) The cumulative probability density function (cdf) of the mean pairwise MN similarity for N=10,000 shuffling repeats, compared to the actual mean. The actual mean is larger than 99.7% of the shuffled instances. (**G**) The bootstrap p-value for the regions of high MN similarity. The two regions with high p-values (Coxa Swing module) are pairs of neurons with small differences in their total synaptic input, such that shuffling the proportional synapses does not degrade a substantial gradient like the gradient that exists for the FETi and SETi in **A**.

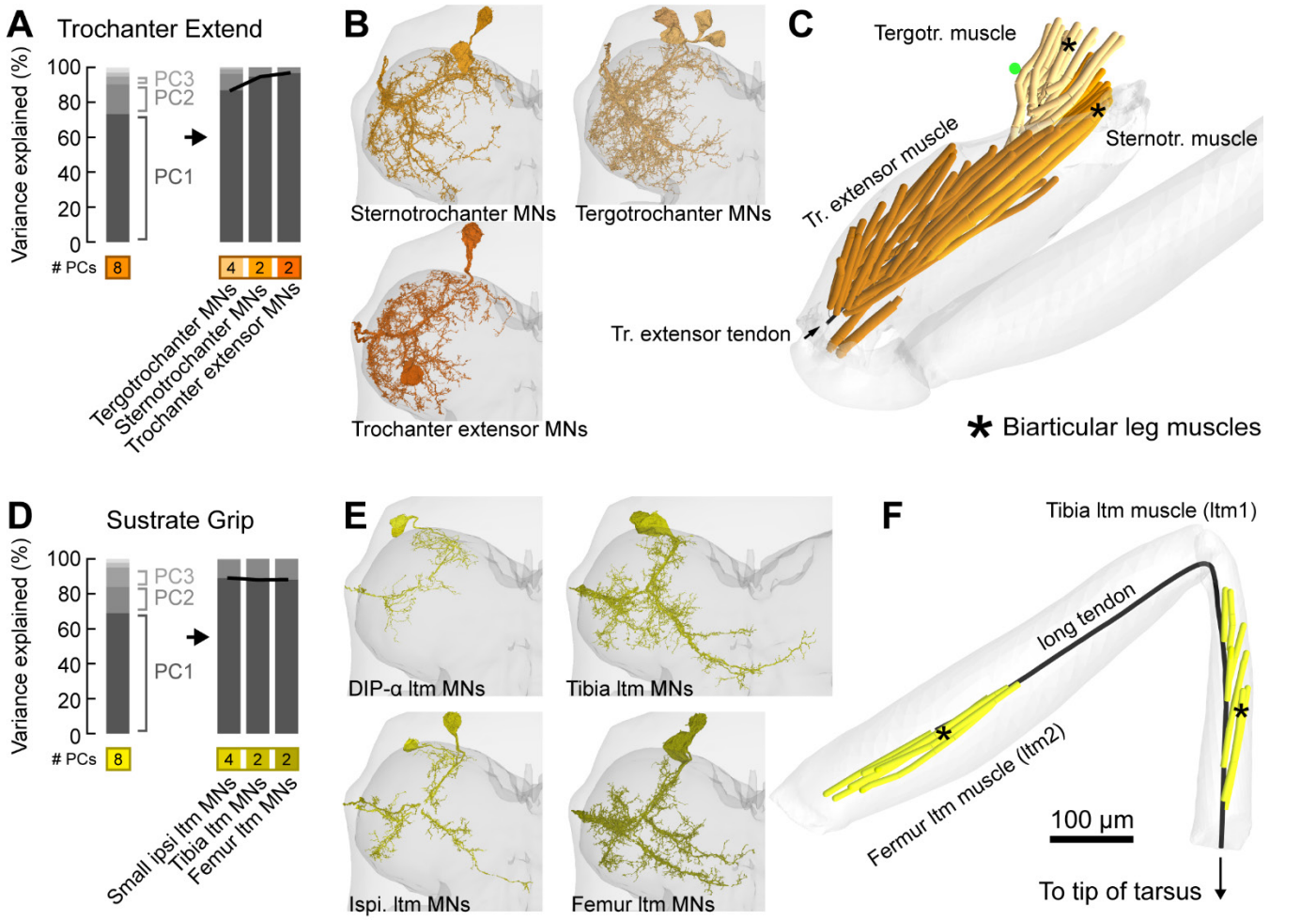

Extended Data Figure 4. Leg modules that include biarticular muscles have more variable module connectivity. (**A**) The first principal component of the module connectivity for the Trochanter Extend module explains less of the variance than for most other leg modules. If the module is separated according to muscle target, the first PC explains more of the variance in the submodule connectivity. (**B**) MNs targeting each muscle. (**C**) The Trochanter Extend module contains the biarticular tergotrochanter muscle, which originates at the dorsal thoracic cuticle (Azevedo et al. 2022), crosses the body-coxa joint and extends the trochanter, and the biarticular sternotrochanter muscle, which originates on the ventral thoracic cuticle, crosses the body-coxa joint and extends the trochanter. (**D**) If the MNs innervating the biarticular long tendon muscle (LTM) are separated by anatomy, the first PC explains more of the submodule connectivity. (**E**) Four groups of ltm neurons. The DIP-α LTM MNs are small, lack a medial projection, express DIP-α, and one targets the femur LTM while the other targets the tibia (Venkatasubramanian *et al.*, 2019). The specific muscle targets of two other smaller LTM MNs are unknown. (**F**) The LTM is composed of two muscles, one in the femur and one in the tibia, that both insert on the long tendon that crosses multiple articulations to insert on the claw at the tip of the tarsus (Radnikow and Bässler, 1991).

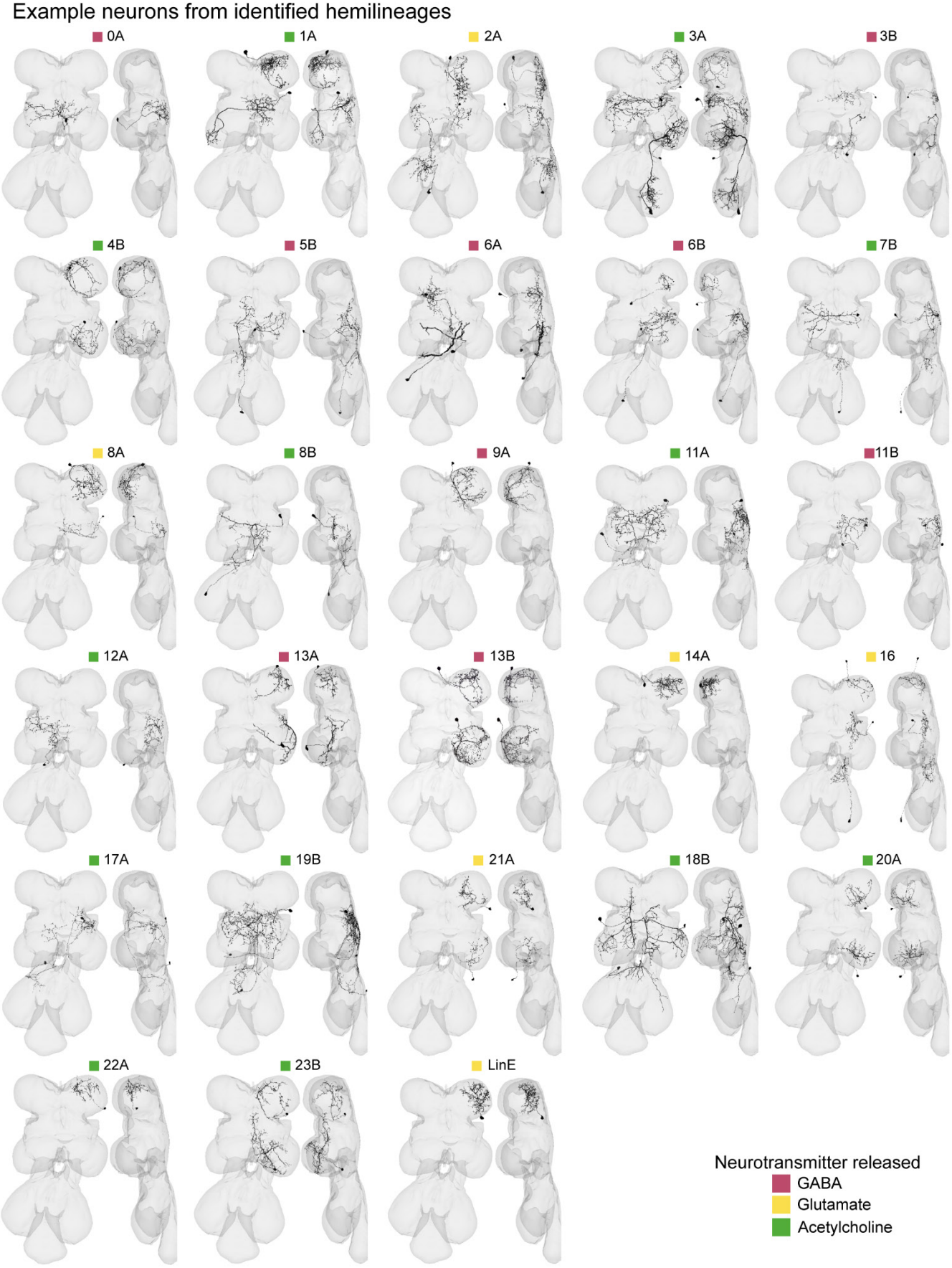
Example neurons from identified hemilineages
0A
1A
2A
3A
3B
4B
5B
6A
6B
7B
8A
8B
9A
11A
11B
12A
13A
13B
14A
16
17A
19B
21A
18B
20A
22A
23B
LinE
Neurotransmitter released
GABA
Glutamate
Acetylcholine

Extended Data Figure 5. Example neurons from each premotor hemilineage. Example preMNs from each premotor hemilineage. See **Supplemental Table 3** for links to view entire premotor populations of each hemilineage in Neuroglancer, an online tool for viewing connectomics datasets.